SLAC – PUB – 4552
February 1988
(T/E)

LIFETIMES OF HEAVY FLAVOUR PARTICLES*

VERA LÜTH

Stanford Linear Accelerator Center
Stanford University, Stanford, California, 94305

ABSTRACT

Measurements of the lifetimes of charm and beauty particles are reviewed, with emphasis on the experimental techniques used for vertex detection.

1. Introduction

In the past few years, decays of hadrons carrying heavy flavour quantum numbers have become a fashionable topic, for theorists and experimentalists alike. In the framework of the standard electro-weak theory, the flavour-changing transitions among quarks and leptons are described by their coupling to the charged weak boson, $W^{\pm}$. The parton diagrams for heavy quarks decay are identical to $\mu^{\pm}$ decay, and thus apart from differences in the couplings of the $W^{\pm}$ to various partons, the semi-leptonic decay rates of the heavy quarks Q are calculable and closely related to the muon decay rate, namely

$$\Gamma(Q \to e^{-}\bar{\nu}_e q) = \frac{G_F^2 m_Q^5}{192\pi^3} |V_{qQ}|^2 \, C(\epsilon)$$

Here G_F is the Fermi constant, and m_Q represents the quark mass. The differences in the couplings of the quarks to the $W^{\pm}$ are given by the Cabibbo-Kobayashi-Maskawa matrix elements V_{qQ}.[1]

In the so-called spectator model, the quarks are treated as being free, there is no flavour mixing and the light valence quarks and gluons do not participate in the decay. The correction function $C(\epsilon)$=1, and the lifetimes of all particles containing a heavy quark Q would be identical, depending only on the quark mass m_Q and the couplings V_{qQ}. In a more realistic case, the function $C(\epsilon)$ depends on the ratio of

* Work supported by the Department of Energy, contract DE-AC03-76SF00515.

to be published in High Energy Electron-Positron Physics
World Scientific Publishing Company

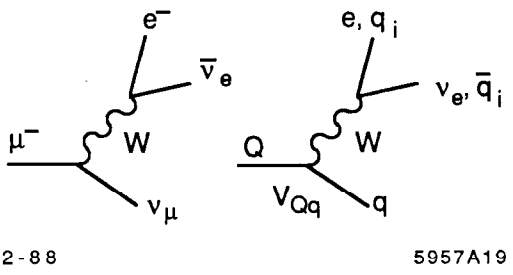

Fig. 1. Diagrams for the β decay of the μ^- and a free heavy quark Q.

the masses of the quarks involved, as well as on the dynamics of the specific decay under study. Precise measurements of the decay rates of heavy flavour mesons and baryons, combined with a detailed study of their branching ratios and decay spectra, can serve as a test of particular models, help to determine the elements of the quark mixing matrix V_{qQ}, and help in the formulation of theoretical models of weak decay.

In this article, lifetime measurements for the charm mesons, D^0, D^+, and D_s^+, the charm baryons Λ_c^+, Ξ_c^+, and Ω_c^0, and beauty hadrons, presumably B^0 and B^- mesons, are reviewed. The report begins with a brief overview of the experimental techniques. The discussion of the theoretical implications of these measurements will be rather brief, and will assume that the reader is familiar with the articles on charm and beauty physics presented in this volume.[2,3]

2. Experimental Techniques

From the point of view of an experimentalist, lifetime measurements are attractive because they represent a major challenge to the design and operation of detectors and to the data analysis. The principal difficulties experimentalists face in the detection of heavy flavour decays are their small production rates in hadron and photon interactions, and their short decay lengths.

Signatures for heavy flavour particles can be derived from their relatively high mass and the weak nature of their decay. Masses of 2 GeV/c^2 and above give rise to large transverse momenta of the decay secondaries, but small branching ratios for any particular decay mode. The weak coupling causes the emission of leptons ($e^\pm, \mu^\pm, \tau^\pm$, and neutrinos) and strange particles due to Cabibbo enhancement. Thus an experiment with good sensitivity requires a large-acceptance spectrometer with excellent momentum resolution and good particle identification, preferentially both for hadrons and leptons, and a vertex detector with superb resolution and granularity. Furthermore, measurements of large numbers of charm and beauty decays are not possible without selective and efficient triggers, or at least the possibility of a fast off-line filter of events.

The difficulty in detecting the characteristic signatures of heavy flavour particles arises from their small production rates. Experimenters have chosen a variety of different beams, operating at energies ranging from threshold to the maximum available. In high energy ν experiments, roughly 10% of the total hadron production by charged current interactions involves charm particles, the total cross section at 100 GeV is, however, of the order of 1pb. In photo-production, the total charm cross section is of the order of a few μb and represents roughly 1% of the inelastic cross section. The highest cross section for charm particle production has been measured in hadron beams, of the order of 10-100 μb/nucleon, but it represents less than 1/1000 of the total inelastic cross section. Beauty cross sections of estimated to be two or more orders of magnitude smaller. The cross sections increase with energy, however, the multiplicity of the hadronic final states increases as well, leading to a higher density of particles in the detectors and a rapidly rising combinatorial background. Typically, there is only one fully reconstructed charm particle decay for every $5 \cdot 10^5$ interactions in a hadron beam, and of the order of one for every 10^4 inelastic photon interactions.

Neutral beam experiments have the advantage that non-interacting beam particles do not register in the detectors, thus allowing for higher beam intensities. This can be a limiting factor for detectors with long sensitivity, like emulsions and bubble chambers. On the other hand, in charged particle beams, the energy and the direction of the incident particles can be very accurately measured. This substantially improves the determination of the interaction point. In fixed target experiments, with the exception on ν beams, the intensity of the beams is adjusted to match the data acquisition capability of the detectors. Much progress has been made in recent years, in the application of micro-processors for selective triggering. Candidate events are selected on-line on the basis of the event characteristics described above, namely high multiplicity and transverse energy, leptons with high transverse momentum, and multiple charged kaons and protons. More recently, several experiments have attempted to detect decay vertices on-line, by reconstructing tracks in arrays of solid state detectors, and by sensing the increase in charged multiplicity downstream of the decay point. So far, the results have not been convincing, but tests are underway to improve these techniques.

Experiments at e^+e^- storage rings have the advantage that 36% of the hadronic final states contain pairs of charm particles, and 9% contain pairs of beauty particles. At the $\Psi(3770)$ and $\Upsilon(10750)$ resonances, the cross sections for D and B meson pairs are enhanced, but the mesons are produced with momenta that are too low to allow for a pathlength measurement. In the continuum above the resonances, i.e. at 15 GeV or more, the cross section for e^+e^- annihilation is less than 1 nb. The total data rate is limited by the luminosity given by the current and cross sections of the stored beams, and not by the data acquisition capabilities of the detectors. In the near future, heavy flavour production can be studied in Z^0 decay at the new colliding beam facilities, SLC at Stanford and LEP at CERN in Geneva. This will be particularly attractive for the study of the decay of beauty

particles for which one expects production rates of 10^6 per year of operation. Experiments measuring e^+e^- annihilation have the clear advantage that samples of charm and beauty events can be selected on the basis of kinematics alone, avoiding losses at short decay distances. One of the major limitations of colliding beam experiments is due to the fact that the production vertex is not observed, but is located somewhere inside the beam-beam interaction region. The use of active targets is clearly not possible. Detectors have to be placed outside a beam pipe of several centimeters in radius and tracks have to be extrapolated over this distance. This is a serious disadvantage, considering that the c.m. energy is relatively low resulting in decay particles of a few GeV momentum and decay lengths of only several 100μm.

The standard method to determine particle decay times is to measure the particle momentum and decay path, and thus requires an accurate determination of the production and decay vertices. If the decay products are not fully detected the momentum is often estimated from an unconstrained kinematic fit or from the measured effective mass and the momentum sum of the measured decay tracks. The accuracy of the estimate is tested by Monte Carlo simulation assuming a specific shape of the production spectrum. A more model independent estimate is based on the study of the decay length measured in the plane transverse to the beam in fixed target experiments. This method uses the fact that the transverse momentum distributions are well known. Another method relies on the measurement of the so-called impact parameter ρ[4] which is defined as the distance of closest approach of a track to the production vertex. ρ is proportional to the product of the decay length and the decay angle, and in the relativistic limit becomes insensitive to the momentum of the decaying particle. The clear advantage of this estimator is that it does not require a fully reconstructed decay or estimate of momentum, and can use individual tracks from hadronic or semi-leptonic decays, thus avoiding unacceptable losses due to small branching ratios and limited detector acceptance. Monte Carlo simulation is needed to relate the impact parameter to the decay time; this can be done to an accuracy of about 10%.

A list of more recent experiments contributing information on heavy flavour lifetimes is given in Table I. Earlier experiments have been described in detail in previous review articles.[5–7] The experiments are grouped according to their methods of vertex detection. Experiments differ widely in their ability to detect secondary vertices, to identify the specific decay modes, and in their data rate capability. Most of these experiments are hybrids which combine fine grained vertex detectors with large downstream spectrometers that provide tracking for charged and neutral particles as well as particle identification.

3. Lifetimes of Charm Particles

In the following, an overview over experiments measuring lifetimes of the charm

Table I: Experiments Measuring Charm and Beauty Lifetimes

The quoted resolution corresponds to the error on the track when extrapolated to the beam interaction point.

Experiment	Resolution (μm)	t_{min} ($10^{-13}s$)	Beam (GeV)	Charged Hadron Identification	Lepton,γ Detection
Emulsions					
WA-75	0.5	0.05	350 π^-	None	$\mu^\pm$
WA-58	1	0.05	50 γ	Cerenkov	Pb glass
E-531	1	0.05	100 ν	TOF	$\mu^\pm$, Pb glass
Bubble Chambers					
NA-18	2	2	340 π^-	None	None
NA-16/27	2.5	1	360 π^-, 400 p	dE/dx,Cerenkov	Pb glass
SHF	7	3	20 γ	Cerenkov	Pb glass
Si-Detectors					
NA-1		2	100 γ	2 Cerenkovs	Pb glass
					Pb scintillator
NA-11/32	8	2	100 π^-	3 Cerenkovs	Pb scintillator
			200 π^-, K^-, p		Cerenkov
NA-14	17	2	100 γ	2 Cerenkovs	Pb glass, $\mu^\pm$
					Pb scintillator
E-691	16	2	145 γ	2 Cerenkovs	$\mu^\pm$, Pb scintillator
					Fe-scintillator
Wire Chambers					
WA-62			135 Σ^-	2 Cerenkovs	None
E-400			650 n	3 Cerenkovs	$\mu^\pm$, Fe-scint.
DELCO	140		29 e^+e^-	Cerenkov	Pb-scintillator
HRS	100		29 e^+e^-	TOF	Pb-scintillator
MAC	90		29 e^+e^-	TOF	$\mu^\pm$,Pb gas
MARKII	95		29 e^+e^-	TOF	$\mu^\pm$,Li-Argon-Pb
JADE	95		35 e^+e^-	TOF, dE/dx	Pb glass
TASSO	90		35 e^+e^-	TOF, 3 Cerenkovs	$\mu^\pm$, Li-Argon-Pb
ARGUS	95		11 e^+e^-	TOF, dE/dx	Pb glass
CLEO	85		11 e^+e^-	TOF, dE/dx	$\mu^\pm$, Pb-scintillator

mesons, D^0, D^+, and D_s^+, (previously referred to as F^+) and charm baryons, Λ_c^+,

Ξ_c^+, and Ω_c^0,* will be given. The experiments are grouped as to the apparatus used for vertex detection.

3.1 Emulsion Experiments

The first candidates for charmed particle decays were observed in 1971 in emulsion chambers that were exposed to cosmic rays.[8] Since then, nuclear emulsions have been revived as active targets for lifetime experiments because of their superb spatial resolution and granularity. Figure 2 illustrates the precision that can be achieved in emulsions, of the order 0.5 μm, corresponding to decay times of down to 10^{-14} s. With the addition of high precision tracking external to the emulsion stacks, computer-aided scanning has substantially enhanced the detection efficiency and data rate capability of this technique. Two experiments have reported results based on data recorded many years ago.

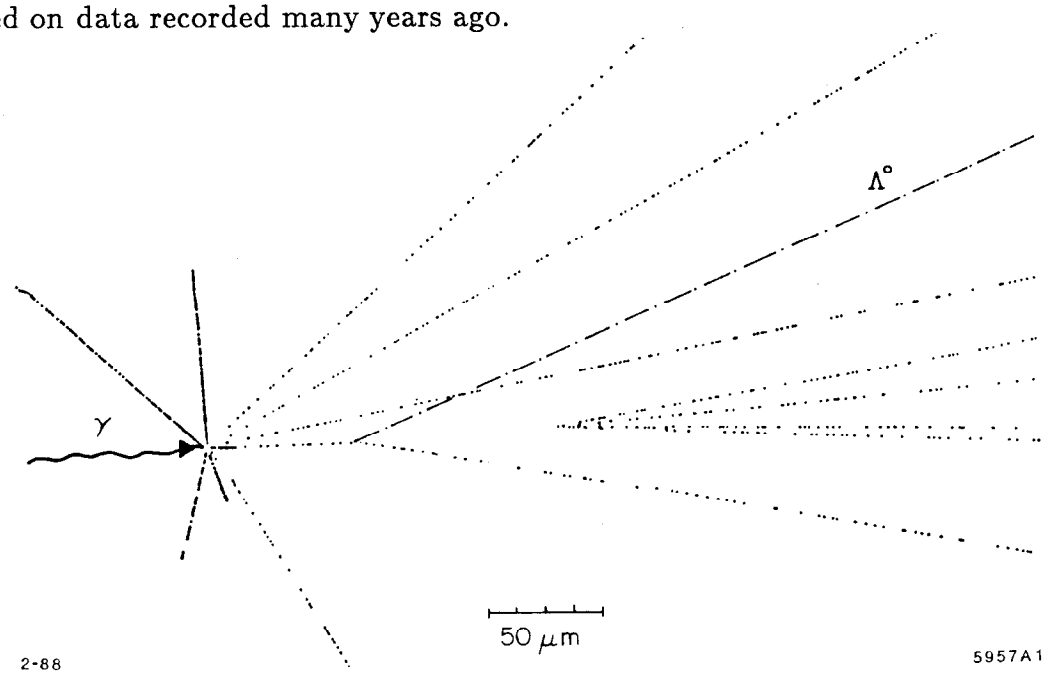

Fig. 2. WA-58: A single event showing the associated photo-production of charm. The event has two decay vertices in the emulsion, $\overline{D}^0 \rightarrow K^+\pi^+\pi^-\pi^-$ and $\Lambda_c^+ \rightarrow \Lambda^0\pi^+$.

3.1.1 FNAL E531 The E-531 experiment[9] employed an emulsion in the ν beam at FNAL. The group published 58 D^0 decays and 47 decays of charged charm particles, among them 6 unique D_s^+ decays, 13 unique Λ_c decays, and 28 decays that are consistent with D^+, but also compatible with the kinematics of D_s^+, and/or Λ_c^+ decay. This Λ_c^+ and D_s^+ contamination, which is estimated from a fit to the decay

* Throughout this report reference to particles like D^0, D^+, D_s^+ implies also the charge conjugate states $\overline{D}^0$, D^-, D_s^-, unless explicitly stated.

time distribution to be 4.8 ± 5.0 events, is responsible for the larger error in the D^+ lifetime. A likelihood fit to the observed decay time distributions results in

$$\tau(D^0) = 4.3 \pm^{0.7}_{0.5} \pm^{0.1}_{0.2} \cdot 10^{-13} \text{ s} \quad \text{and} \quad \tau(D^+) = 11.1 \pm^{4.4}_{2.9} \cdot 10^{-13} \text{ s}.$$

The ratio of these two lifetimes is $2.6 \pm^{1.1}_{0.8}$. The average lifetimes of the fitted D_s^+ and Λ_c^+ decays are $2.6 \pm^{1.6}_{1.1} \cdot 10^{-13}$ s and $2.0 \pm^{0.7}_{0.6} \cdot 10^{-13}$ s, respectively.

3.1.2 CERN WA-58 The WA-58[10] group exposed a thin emulsion target in the Ω spectrometer to a photon beam at the CERN SPS. Their results, listed in Tables III and IV, are based on 45 events containing 27 D^+, 44 D^0, and 11 Λ_c^+ decays. While the observation of two secondary vertices per event greatly enhances the purity of the charm selection, the identification of individual decay modes remains difficult, partially due to the limited mass resolution and particle identification of the spectrometer. Only 8 D^+, 8 D^0, and 2 Λ_c^+ decays are identified by unambiguous fits to decay modes involving two or more charged and no neutral secondaries. Furthermore, the limited thickness of this emulsion stack leads to substantial corrections for detection losses at proper times exceeding $3 \cdot 10^{-13}$ s.

3.2 Bubble Chamber Experiments

The use of bubble chambers as active targets has the advantage that within a small fiducial volume, tracks can be scanned with high efficiency, accurately measured and clearly associated with the production or decay vertices. The single track resolution has been substantially improved by the introduction high resolution optics and monochromatic light, by improved measuring machines, and by optimum operating conditions resulting in small bubble diameters and high bubble density. At Fermilab, holography is being used in the 15 feet bubble chamber.

3.2.1 SLAC Hybrid Facility At SLAC, a total of $2.4 \cdot 10^6$ pictures were taken by the 1m long bubble chamber of the Hybrid Facility in the 20 GeV back-scattered laser beam.[11] The bubble chamber was backed by two threshold Cerenkov counters, a lead-glass calorimeter and wire chambers. In addition to three stereo view cameras, the set-up was equipped with one high resolution camera. The experimenters rely on the excellent vertex resolution and picture quality to select a sample of clean charm decays by visual observation. The bubble size was adjusted to be of the order of 50 μm, the density roughly 60 bubbles/cm. To obtain high and uniform detection efficiency ($97 \pm^{2}_{4}\%$) and to reduce topological ambiguities at short decay lengths, a minimum pathlength of 600 μm, one decay track with an impact parameter of at least 100 μm and a second one with at least 40 μm were required. After additional cuts to remove photon conversions and strange particles, 100 charm decays remain, 50 D^0, 48 $D^{\pm}$, and two ambiguous decays. There is no direct evidence for D_s^+ or Λ_c^+ decays. Only one-third of the decays can be kinematically constrained, because of unmeasured neutral particles, π^0 and ν. The momentum of the decaying charm mesons is derived by scaling from the visible momentum p_{vis} and effective mass m_{vis},

namely $p_D = p_{vis}(m_D/m_{vis})$. The efficiency corrected decay time distributions are shown in Figure 3. The best fit results in

$$\tau(D^0) = 6.1 \pm 0.9 \pm 0.3 \cdot 10^{-13}\ \text{s} \quad \text{and} \quad \tau(D^+) = 8.6 \pm 1.3 \pm^{0.7}_{0.3} \cdot 10^{-13}\ \text{s}.$$

and

$$\tau(D^+)/\tau(D^0) = 1.4 \pm 0.3 \pm {}^{0.2}_{0.1}.$$

The quoted systematic errors include the uncertainty in the momentum and efficiency estimates, and the error due to a small possible contribution from Λ_c^+ and D_s^+ decays to the D^+ sample. In both, the D^0 and the D^+ sample, there is one event with a rather long decay time. In particular, the neutral decay with $\tau = 55 \cdot 10^{-13}$s is a well measured and fully constrained decay with an extremely low probability of being background. Even though the statistical probability for the observation of such an event is low ($6 \cdot 10^{-4}$ for an average lifetime of $4.4 \cdot 10^{-13}$s) the authors stress the fact that the data sample is fully consistent with an exponential decay distribution.

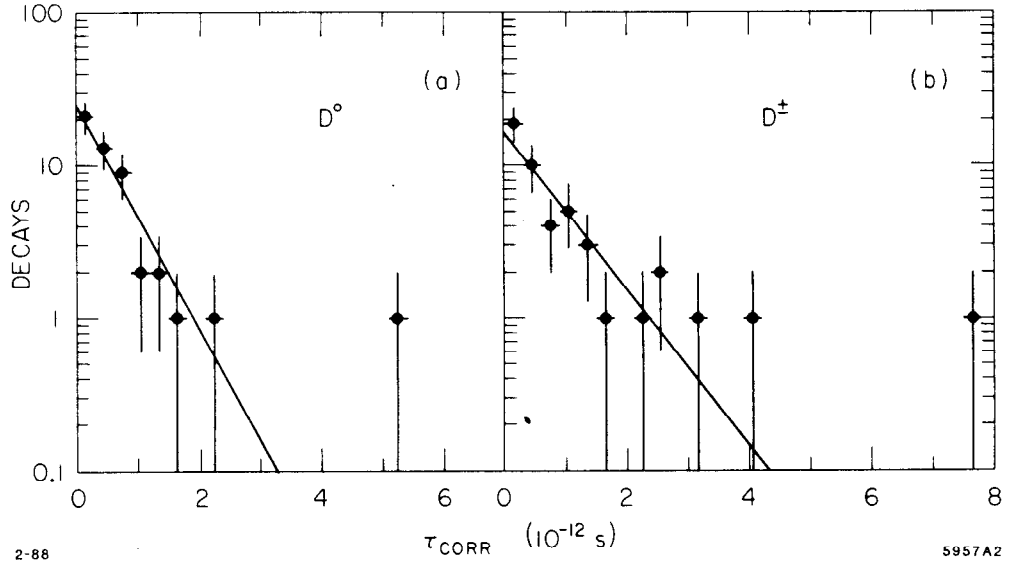

Fig. 3. SHF: Corrected decay time distributions for a) 50 D^0 and b) 48 $D^\pm$ decays.

3.2.2 CERN NA-27 The NA-27 group used the small hydrogen bubble chamber, LEBC, in the European Hybrid Spectrometer and has recently completed the analysis of data from exposures in a 360 GeV π^- beam and a 400 GeV proton beam.[14] Following the event selection by two independent scans, the tracks were recorded by a High Precision Measuring Device (HPD). Figure 4 shows a candidate for charm pair production as digitized by the HPD. A typical track of 5 cm length has roughly 400 precisely aligned bubbles of less than 20 μm diameter. The bubble

centers are located with a precision of 5 μm resulting in rms residuals of 1.8 μm for approximately 25 points. The resolution in the impact parameter was found to be better than 2.5 μm, allowing for efficient detection of all tracks with impact parameters of 10 μm or more.

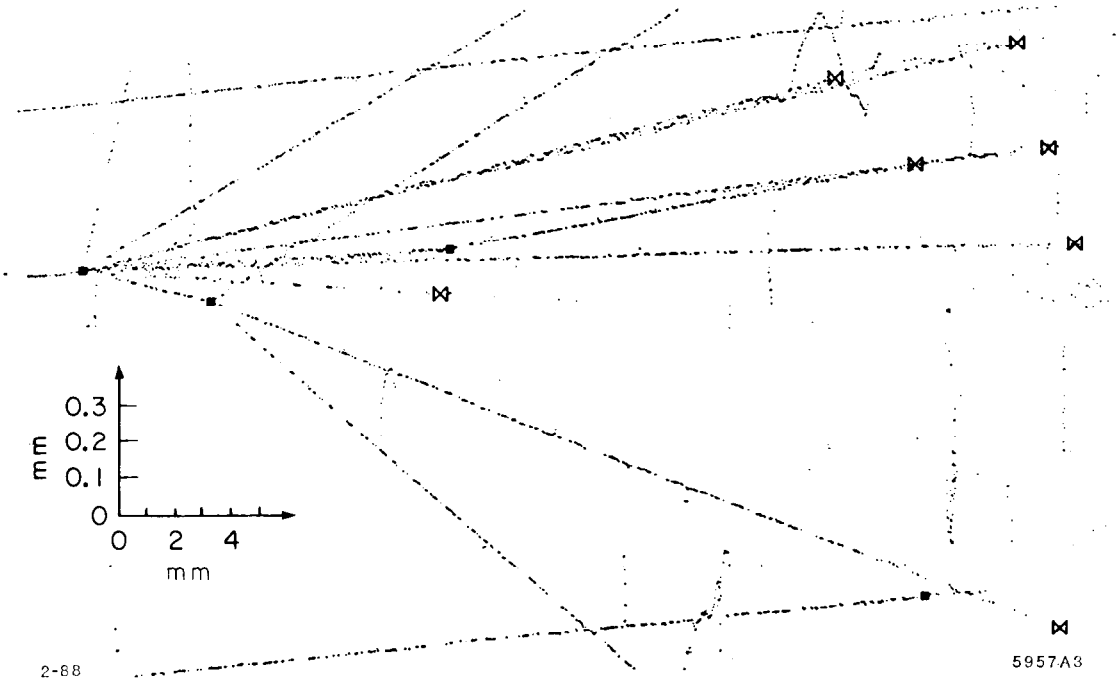

Fig. 4. NA-27: Digitization of an event with two decay vertices by the HPD. Note the different scales parallel and transverse to the beam direction.

Charm events are required to have one or more tracks that do not point back to the main vertex. In total, 438 events are selected with 664 detected charm decay vertices of multiplicity two or more. All decays are passed through kinematic reconstruction, subject to all mass assignments compatible with the particle identification. K^o and Λ^o decaying in the spectrometer as well as π^o candidates found in the photon detectors are considered. 64 D^+ and 53 D^o decays give good fits. For these events, the decay time is determined from the decay length and the fitted momentum.

For those charm decays that cannot be constrained by kinematics, the experimenters have tried several different methods to derive lifetime estimates.[15] In particular, they have introduced a technique that reduces the model dependence and can be applied to both constrained and selected unconstrained decays. The distribution of decay lengths, $l_\perp$, measured in the plane transverse to the beam is combined with the measured transverse momentum distribution. The $p_\perp^2$ distribution is well described by an exponential function of the form

$$\frac{d\sigma}{dp_\perp^2} = a\ exp(-bp_\perp^2)$$

with b=$1.18\pm^{0.18}_{0.16}$ for both charged and neutral D mesons.

Maximum likelihood fits were performed separately for the π^- and proton data, for all events using the transverse decay length and the $p_\perp$ distribution, and for decays which are kinematically fit using the fitted momentum and the total decay length. The different methods and data sets give compatible results. The authors quote a combined result,

$$\tau(D^0) = 4.6 \pm^{0.6}_{0.5} \cdot 10^{-13} \text{ s} \quad \text{and} \quad \tau(D^+) = 11.2 \pm^{1.4}_{1.1} \cdot 10^{-13} \text{ s}.$$

The ratio of D^+ to D^0 lifetimes is 2.4±0.4. By applying different techniques to measure lifetimes to different, but overlapping event samples the authors conclude that the transverse decay length is a robust estimator of the lifetime. The 15% uncertainty in the parameter b defining the transverse momentum distribution results in an 8% systematic error in the lifetimes. It is included on the quoted error.

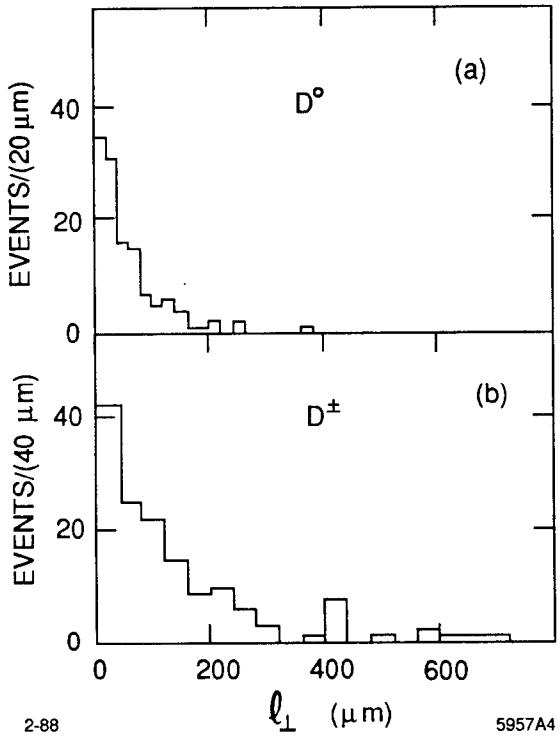

Fig. 5. NA-27: Transverse decay length distributions for selected D meson decays.

The transverse decay length distributions for 145 D^o and 149 D^+ decays are shown in Figure 5. The length $l_\perp$ has been corrected, event by event, for the minimum detectable length. The two distributions are clearly different, the average transverse lengths are 59 μm and 140 μm. In the D^+ sample, there is no evidence for a short-lived component due to D_s^+ or Λ_c^+ contamination.

The NA-27 has also reported a result[16] on the Λ_c^+ lifetime, based on nine three-prong vertices that have been unambiguously fitted to Cabibbo-favoured decay modes, $\tau(\Lambda_c^+) = 1.2 \pm^{0.5}_{0.3} \cdot 10^{-13}$ s.

3.3 Experiments with Silicon Vertex Detectors

Given the limitations of nuclear emulsions and bubble chambers, e.g. long sensitivity, limited data rate capability, and difficult scanning procedures, a major effort has been devoted to developing silicon detectors with finely segmented electrodes for charge collection. Such detectors represent an outgrowth of the semiconductor counters that have been used in nuclear physics for more than twenty years. In high energy physics, the use of Silicon as an active target and as a high resolution tracking device was pioneered by two groups at CERN, NA-1[17] and NA-11.[18] Since then, many other experimenters have built on this experience and have employed commercially available Silicon detectors with strip and pixel read-out.

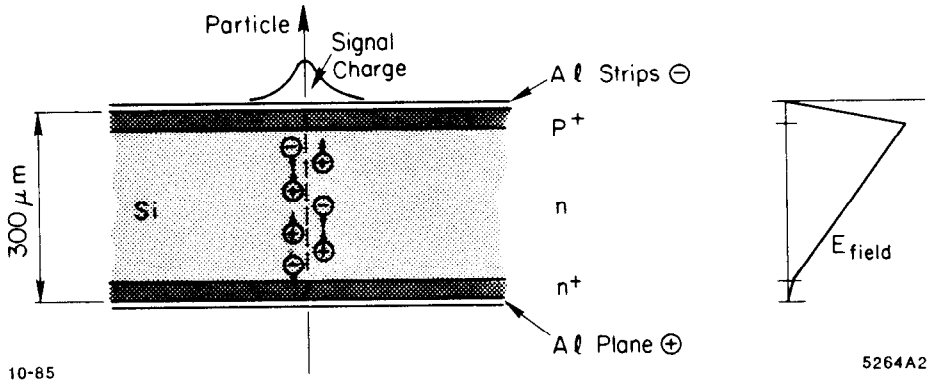

Fig. 6. Schematic lay-out of a silicon strip detector.

Silicon detectors are made from wafers of high resistivity (typically $5k\Omega$ or more) mono-crystals. Figure 6 shows the cross section of a typical micro-strip detector made from n-type silicon wafers, 2-4 inches in diameter and about 300 μm thick. On the backside of the counter, there is a thin metal contact, deposited on a n^+ implant. On the top, the counter has p^+ implanted diode strips covered with aluminium contacts, typically less than 10 μm wide for a 20 μm pitch. Connecting the backplane to a positive voltage of 100V or less depletes the n-doped crystal of free charge carriers and leaves dopant concentrations of the order of $10^{13} \cdot cm^{-3}$ atoms which produce an electric field that decreases linearly with distance from the junction. A minimum ionising charged particle traversing the detector produces roughly 80 electron-hole pairs per μm in a narrow column around the particle's path. This is due to the narrow band gap of 1.1 eV resulting in only 3.6 eV of energy loss per pair and due to the short range of electrons and photons, typically 1 μm for a 15 keV electron. The produced charges drift in the electric field towards the metal strips. For a pathlength of 300 μm, typical collections times are 10-20 ns. The increase in transverse spread of the charges due to diffusion is about 8 μm for

electrons and 5 μm for holes. The lifetime of the charge carriers, typically several ms, strongly depends on the details of the specifications and the fabrication process.

Detectors vary greatly in their dimensions, some have up to thousand strips, the minimum pitch realised so far is 20 μm, the maximum length is 90 mm. Various read-out methods have been used, depending on the spatial resolution and two-particle separation required. Most experiments use analog pulseheight information and determine the exact position of the particle trajectory by a pulseheight weighted mean of the strip coordinates. Spatial resolutions of better than 3 μm have been achieved.

To reduce the number of read-out channels, several experiments use capacitive coupling. By developing low noise analog electronics and by sputtering the strip detector with amorphous silicon, spatial resolutions of 4.5 μm and 20 μm have been measured with 20 μm strip spacing, for read-out pitches of 60 μm and 240 μm respectively.[19] Resistive charge division has been frequently used in nuclear physics for the detection of heavy ions in rather thick detectors. Its application in high energy physics appears to be difficult, given the low noise level required for minimum ionising particles and detector thicknesses of 300 μm or less.

The main drawback of finely segmented arrays of silicon micro-strip detectors has been up to now the large volume and cost of the read-out electronics. In recent years several groups have been developing custom designed VLSI circuits that contain the electronics for a large number of channels on a few mm^2.[20–22] The first example for such a circuit is the "Microplex" chip[20] which contains low noise amplifiers, analog storage and multiplexed read-out for 128 channels.

An alternative to the one-dimensional strip read-out are pixel devices, like Charged Coupled Devices (CCD) which store the charge in two-dimensional potential wells. Read-out of large arrays of such pixels is by sequential clocked transfer of the stored charge, row by row, and column by column, to a single charge amplifier. Typical pixel sizes are 22 μm x 22 μm in arrays of several cm^2. The shallow depletion depth of 12 μm results in only about 1000 charge carriers per minimum ionising particle and makes cooling of these devices mandatory. On the other hand, this shallow depth prevents a degradation of performance for non-normal incidence which is observed for the much thicker strip detectors. This problem is caused by the fact that in this situation the direction of the drift is at an angle to the track and consequently the charges are collected over many narrow strips.. The problem could be overcome by a substantial reduction in noise and/or reduction in the thickness of the depletion region. The disadvantage of the CCDs is the rather long read-out time. Developments are under way to increase the speed by orders of magnitude to 300 Mhz.[23,24]

3.3.1 CERN NA-1 The NA-1 experiment[25,26] was operated in the CERN photon beam and recorded $5 \cdot 10^6$ triggers. The target was made of 40 silicon wafers (with no segmentation of the electrodes), 300 μm thick and spaced by 100 μm to detect

multiple vertices in an event by means of an increase in ionisation in downstream wafers. The technique is illustrated in Figure 7. It is best suited to coherent charm production, in which the highly ionising target disintegration products are avoided, and to photo-production at moderate energies where the primary multiplicities are moderate and thus there is sensitivity to small changes in ionisation. Still, there are problems due to Landau fluctuations and secondary interactions and photon conversions. Also, since there are two charm decays per event, the association of the decay length and the charged decay secondaries often remains ambiguous. This problem has been overcome by selecting exclusive $D^0\overline{D}^0$ production and $D^{*+} \rightarrow D^0\pi^+$ decays, or by requiring that there is only one decay vertex of multiplicity two in the event. In a recent publication[27] the NA-1 collaboration presented a sample of 9 decays $\Lambda_c^+ \rightarrow K^-\pi^+ p\,\pi^0$, one of which is also compatible with a D_s^+ decay. The average lifetime of the selected decays is $\tau(\Lambda_c^+) = 1.1 \pm^{0.8}_{0.4} \cdot 10^{-13}$ s. The number of background events is quoted to be of the order of one, no events of the decay to $K^-\pi^+ p$ or any other Λ_c^+ decay mode have been observed.

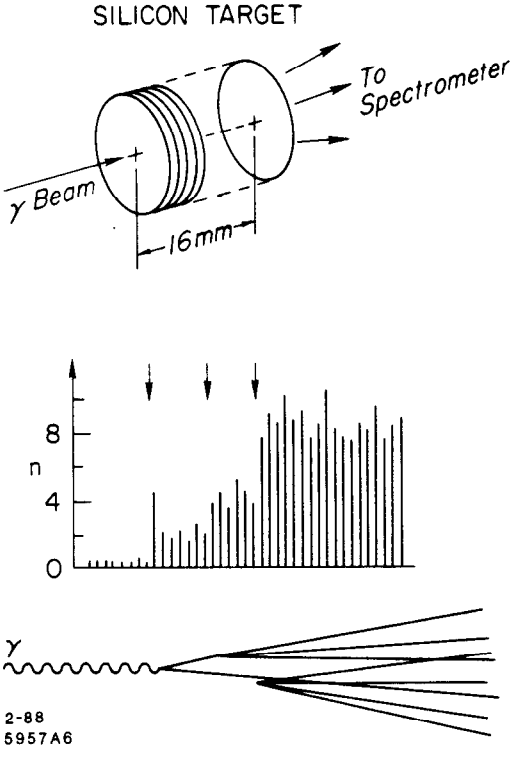

Fig. 7. NA-1: The use of Silicon wafers as an active target, a) layout, b) pulseheight versus wafer number for an event with the decay of two charm particles in the target as sketched in c).

The NA-14 group has recorded 17 10^6 events in a high resolution spectrometer in the CERN tagged photon beam. The vertex detector consists of 10 planes of

silicon microstrip detectors and an active target with transverse segmentation. Very promising preliminary results on D^0 and Λ_c^+ lifetimes are now available.[28]

3.3.2 CERN NA-11 The NA-11 group developed the first silicon microstrips and employed them to reconstruct secondary vertices.[29] A telescope of seven Silicon microstrip detectors with capacitive charge division read-out was placed a few cm downstream of the target and upstream of a large, high resolution spectrometer. Six of the counters were arranged in pairs with strips at an angle of ± 14 degrees to the horizontal plane, a seventh counter was placed with its strips horizontal. Six small microstrip counters in front of the berylium target measured the position of the incident beam to a few μm. An event with two charm particle decays is shown in Figure 8. The single track resolution is 5 μm, the efficiency was measured to be $> 99\%$. A system of on-line processors was used to trigger on prompt electrons or more than one kaon, detected by a calorimeter and Cerenkov counters downstream.

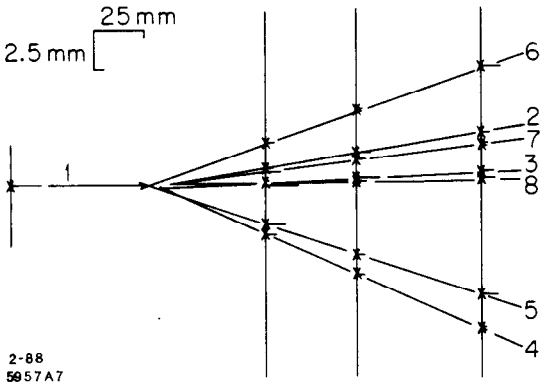

Fig. 8. NA-11: A charm event as observed in the silicon strip vertex detector. Tracks 2,7,and 8 originate from an D_s^+ decay, tracks 3 and 5 from a $\overline{D^0}$ decay.

The selection of charm decays relies heavily on the microstrip telescope and is restricted to fully reconstructable decay modes, $D^0 \rightarrow K^-\pi^+, K^-\pi^-\pi^+\pi^+$ and $D^+ \rightarrow K^-\pi^+\pi^+$. The decay tracks are required to form a distinct vertex, the kaons are identified by Cerenkov counters. The final sample consists of 33 D^+ and 29 D^0 decays, including 5±2 and 3±1 background events.[30] While the statistics of this sample is not impressive, its cleanliness is. This experiment proved that silicon microstrip detectors can be built to detect minimum ionizing particles, and that they can be used to isolate extremely pure samples of charm decays, and thus make possible not only measurements of lifetimes but also studies of production mechanisms of charm and - in the near future - beauty particles in photon and hadron interactions. Details of the analysis are given below. The data are corrected for detection losses and background, and then fit by a maximum likelihood method. The results are listed in Table III. In addition, the group has presented a sample of

69 semi-leptonic decays $D^+ \to \overline{K}^{*0}(890)\ e^+\nu_e$.[31] The decay times are estimated using the observed invariant mass and momentum, and corrected for the minimum detectable decay time compatible with the vertex cuts. The resulting lifetime of $\tau(D^+) = 11.2 \pm^{1.6}_{1.3} \pm 0.8 \cdot 10^{-13}$ s compares well with the result based on hadronic decays.

3.3.3 CERN NA-32 In an attempt to detect secondary vertices at the trigger level, the same group, under the label NA-32, installed an active target of 14 finely segmented silicon counters with analog read-out.[32] While the on-line charm selection did not produce satisfactory results, a total of $38 \cdot 10^6$ were recorded with an interaction trigger in a 200 GeV hadron beam. At present 22 million π^- and 5 million K^- interactions have been analysed resulting in 149 fully reconstructed D decays. The required background separation of 10^5 is achieved by a series of cuts that rely on the excellent spatial resolution of microstrip vertex detector. Two or more tracks are required to from a vertex that is separated from the interaction point by a distance of more than 2 mm for D^o and 3 mm for D^+. In addition, the impact parameters of at least two decay tracks have to be larger than the resolution by 3 σ, all of them have to exceed 1 σ, where σ refers to the estimated error in the impact parameter. The D momentum must point back to the production point to within a few μm.

Signals from three threshold Cerenkov counters were employed to identify and separate specific decay modes. All candidate events were checked for consistency with charm decay by a scan of the active target pulseheight information. Vertices were identified by an increase in the track multiplicity, secondary interactions were flagged by very large clusters in pulseheight. The data, shown in Figure 9, demonstrate the cleanliness of the samples. There are 59 $D^+ \to K^-\pi^+\pi^+$ decays, 58 $D^0 \to K^-\pi^+$ and 32 $D^0 \to K^-\pi^-\pi^+\pi^+$ decays, above backgrounds of 1.5 and 1.9 and 2.2, respectively. Maximum likelihood fits to the background subtracted time distributions yield

$$\tau(D^0) = 4.2 \pm 0.5 \cdot 10^{-13} \text{ s} \qquad \text{and} \qquad \tau(D^+) = 10.9 \pm^{1.9}_{1.5} \cdot 10^{-13} \text{ s}.$$

The systematic errors are estimated to be substantially smaller than the statistical errors quoted. The measurements translate into a lifetime ratio of $\tau(D^+)/\tau(D^0) = 2.6 \pm 0.5$.

The NA-32 group[33] has applied the same analysis to search for the decay $D_s^+ \to K^-K^+\pi^+$ and finds 12 events above a background of less than one. Due to ambiguities in the kaon and proton identification, a few events are compatible with the decay modes $D^+ \to K^-\pi^+\pi^+$ or $\Lambda_c^+ \to K^-p\pi^+$. They are excluded from the sample. A fit to the corrected decay time distribution gives $\tau(D_s^+) = 3.4 \pm^{1.3}_{0.9} \cdot 10^{-13}$ s. In the NA-11 sample, the same group has isolated 9 D_s^+ decays resulting in a fitted lifetime of $\tau(D_s^+) = 3.2 \pm^{1.5}_{1.0} \cdot 10^{-13}$ s. If we combine these 9

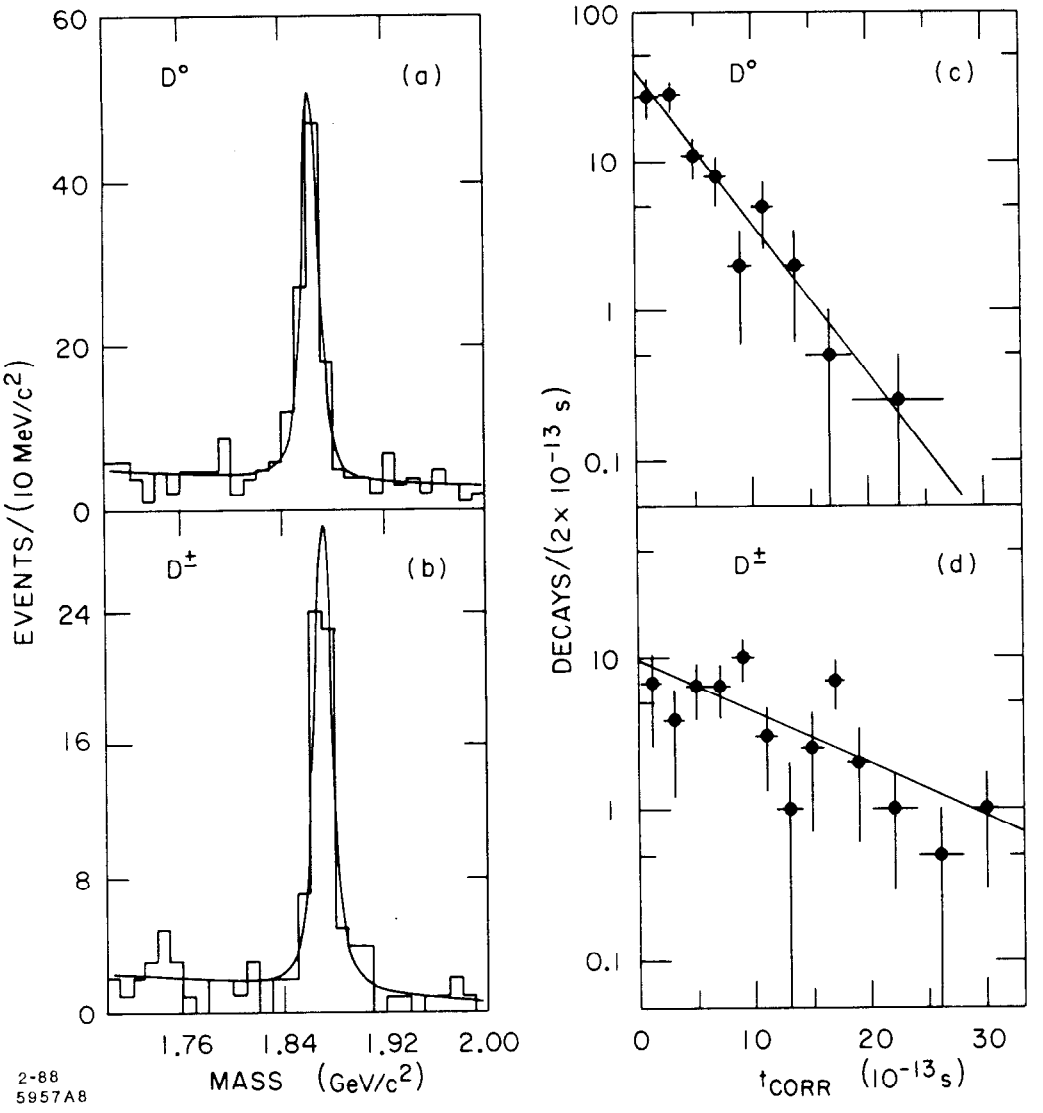

Fig. 9. NA-32: Effective mass and corrected decay time distributions for the selected D mesons decays.

decays with the 12 decays observed by NA-32 the weighted average is

$$\tau(D_s^+) = 3.3 \pm {}^{1.0}_{0.6} \cdot 10^{-13} \text{ s}.$$

The mass of the D_s^+ is $1972.7 \pm 1.5 \pm 1.0\ MeV/c^2$.

In 1985 the NA-32 collaboration improved the resolution and granularity of the vertex detector by the addition of two CCDs at a distance of 10 mm and 20 mm from a 2.5 mm thick Cu target, that was exposed to a 230 GeV negative hadron beam. The trigger required at least two particles without a signal in the threshold Cerenkov counters, thus increasing the D_s^+ and Λ_c signals by about a factor of 3. This is the first use of Charged Coupled Devices as tracking detectors for minimum ionizing particles. With this set-up, the resolution of the tracks extrapolated to the beam

interaction point is measured with a precision (in μm) of $\sigma^2 = 5^2 + (18/p)^2$, where the first term gives the intrinsic resolution of the set-up, the second term represents the contribution from multiple scattering. The primary vertex is determined with a precision of $\sigma_x \approx \sigma_y \approx 2$ μm in the transverse plane and $\sigma_z \approx 60$ μm in the direction of the incoming beam. This remarkable performance results in a very clean separation of the secondary vertices. At present roughly 60% of the 16 million triggers have been processed and preliminary results have been presented at recent conferences.[34,35]

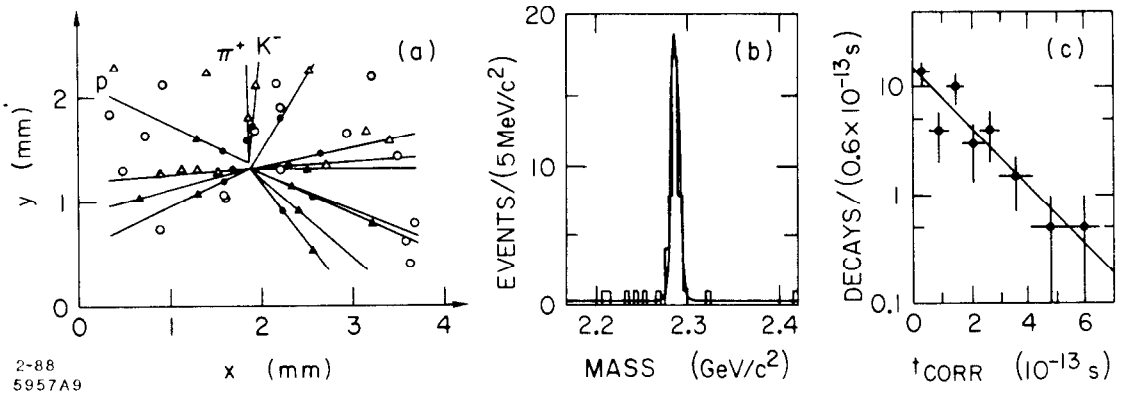

Fig. 10 NA-32: Measurement of the Λ_c lifetime, (a) display of a single event detected by the CCDs in the projection transverse to the beam, (b) effective mass and (c) decay time distribution. Hits in the first and second CCD are marked as triangles and circles, respectively. The open symbols mark hits that are not associated with this event. They are due to additional beam tracks passing during the active time of the CCDs.

Figure 10a shows a decay $\Lambda_c^+ \rightarrow pK^-\pi^+$ as observed in a plane parallel to the CCDs. With an incident intensity of 10^6 particles per 2.5 s beam pulse, there are on average 2 hits/mm^2, compared to a cell density of 2100/mm^2 in the active area of 8.8×2.4 mm^2. A total of 40 Λ_c decays have been observed. Their masses peak at 2287.2 ± 0.6 MeV/c^2. Three decays with ambiguous particle identification are compatible with D^+ or D_s^+ decay to $KK\pi$ and they are excluded from the lifetime determination. A fit to this practically background free sample gives

$$\tau(\Lambda_c^+) = 1.6 \pm {}^{0.4}_{0.3} \pm 0.3 \cdot 10^{-13} \text{ s},$$

where the systematic error reflects the sensitivity of the fit to changes in the event selection and assumed position error.

A very similar analysis leads to the selection of 20 D_s^+ decays and a fitted lifetime of $\tau(D_s^+) = 4.5 \pm^{1.9}_{1.1} \cdot 10^{-13}$ s. No systematic errors are given at this time.

3.3.4 FNAL E-691 The most precise measurements of charm particle lifetimes have been reported by the E-691 group from Fermilab.[36,37] This group built on

the experience of earlier experiments. It combined the high data rate ability of the Fermilab Tagged Photon Spectrometer with the excellent resolution of by now commercially available silicon microstrip detectors. The spectrometer is shown in Figure 11. During a three month period in 1985, a total of 10^8 inelastic interactions in the 5 cm long beryllium target were selected by a trigger on the transverse energy measured in the downstream calorimeters. With a threshold of 2.2 GeV, this trigger rejected 70% of all hadronic interaction while retaining 80% of the events with charm decays. The photon energy spectrum extended from 90-260 GeV, the mean tagged photon energy was 145 GeV. Three triplets of silicon microstrip detectors with 50 μm spacing and digital read-out were installed to improve the charged particle tracking close to the target. Each triplet had three strip orientations, $X(0^o), Y(90^o)$, and $V(-20.5^o)$. The angular acceptance was about 100 mrad.

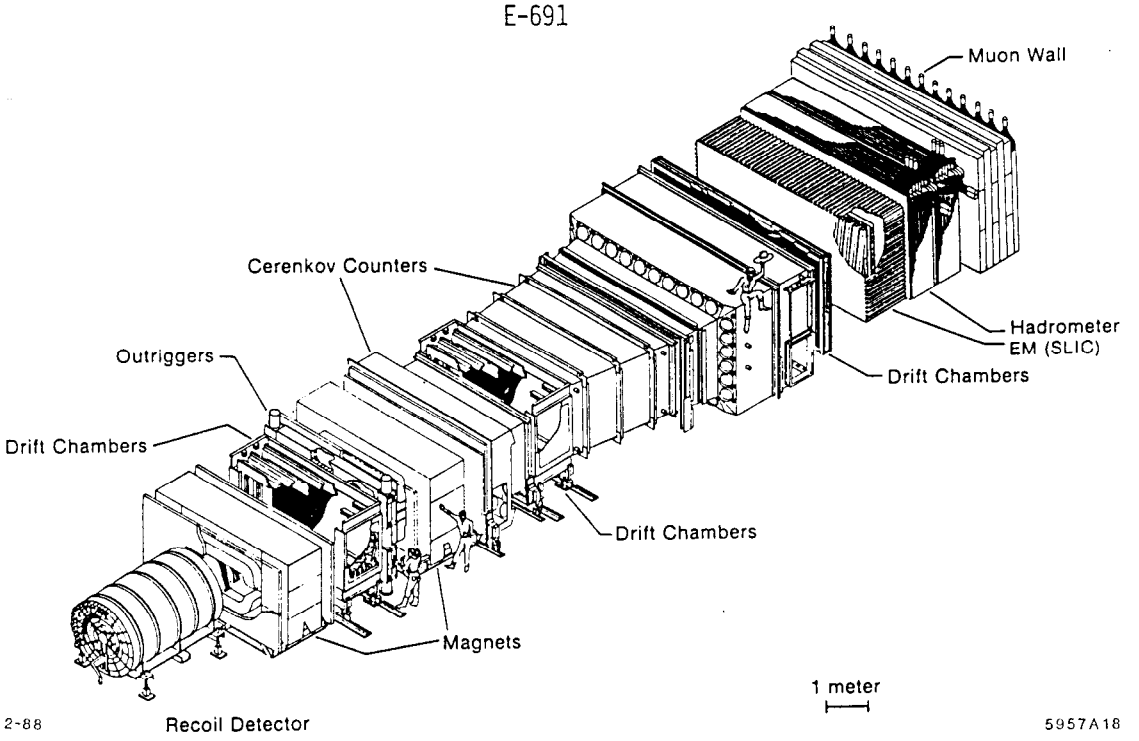

Fig. 11. E-691: Plan view of the Tagged Photon Experiment at FNAL.

Since the transverse decay lengths exceed the intrinsic resolution of the silicon detectors of 14 μm by about a factor of 10, about half of the charm decays vertices can be resolved from the beam interaction point. The event selection is remarkably straightforward. It relies heavily on the silicon detectors that are placed in the field-free region in front of the first magnet. It is designed to minimize systematic errors in the determination of the lifetimes. (1) Tracks from the decay of a charm particle are required to form a good secondary vertex, all other tracks are used to form the primary vertex. (2) The impact parameter of the reconstructed charm candidate relative to the primary vertex is not to exceed 80 μm. (3) The particle masses have

to be consistent with the Cerenkov counter pulse heights. (4) To further reduce the non-charm background, only charm candidates are kept that decay at least a longitudinal distance z_{min} downstream of the primary vertex. This distance z_{min} is chosen to be 6-10 times the resolution σ_z, depending on the decay mode. The value of σ_z is typically 300 μm for a D momentum of 60 GeV/c, corresponding to a proper time resolution of 0.03 ps. The ratio z/σ_z and the proper time resolution are essentially independent of momentum. The proper time t is calculated using the measured momentum and the decay distance l corrected for the cut on z_{min},

$$t = 1/\gamma\beta c \cdot (l - l_{min}),$$

where l_{min} is the distance in the flight direction corresponding to z_{min}.

Table II: Results from Experiment E-691 at FNAL

Decay Mode	Vertex Cut z_{min}/σ_z	Decays	Background	Lifetime (10^{-13} s)
$D^o \to K^-\pi^+$	8	2303 ± 48	768 ± 14	4.20 ± 0.11
$D^{*+} \to D^o\pi^+ \to K^-\pi^+\pi^+$	5	1210 ± 36	94 ± 5	4.17 ± 0.14
$D^{*+} \to D^o\pi^+ \to K^-\pi^+\pi^+\pi^-\pi^+$	7	700± 27	113 ± 5	4.37 ± 0.19
$D^+ \to K^-\pi^+\pi^+$	10	2992 ± 55	1383 ± 20	10.9 ± 0.3
$D_s^+ \to \phi\pi^+$	7.5	143 ± 14	49 ± 4	$4.5 \pm {}^{0.5}_{0.4}$
$D_s^+ \to \overline{K}^{*o}K^+$	10	85 ± 11	26 ± 3	$4.9 \pm {}^{0.8}_{0.6}$
$\Lambda_c^+ \to pK^-\pi^+$	8	97 ± 14	91 ± 10	$2.2 \pm {}^{0.3}_{0.2}$

The resulting four D meson samples are presented in Figure 12 and Table II. There are three samples for the D^0 and one for the D^+, their statistics is remarkable. The lifetimes τ are determined by a maximum likelihood fit to a sum of signal and background,

$$N(t) = N \cdot f(t)\ e^{-t/\tau} + b(t),$$

where $b(t)$ is the proper time distribution of the background, as determined from events above and below the D peak in the mass plot. The function $f(t)$ is obtained by Monte Carlo simulation, it corrects for the effects of acceptance, resolution, and efficiency, including losses due to absorption of decay particles in the target. The free parameters in the fit are N, the total number of charm decays, and τ, the lifetime. The results of the fits are given in Table II. The three D^0 samples are statistically independent, they have different corrections and background. The fact that all three samples agree provides a check on the consistency of the method.

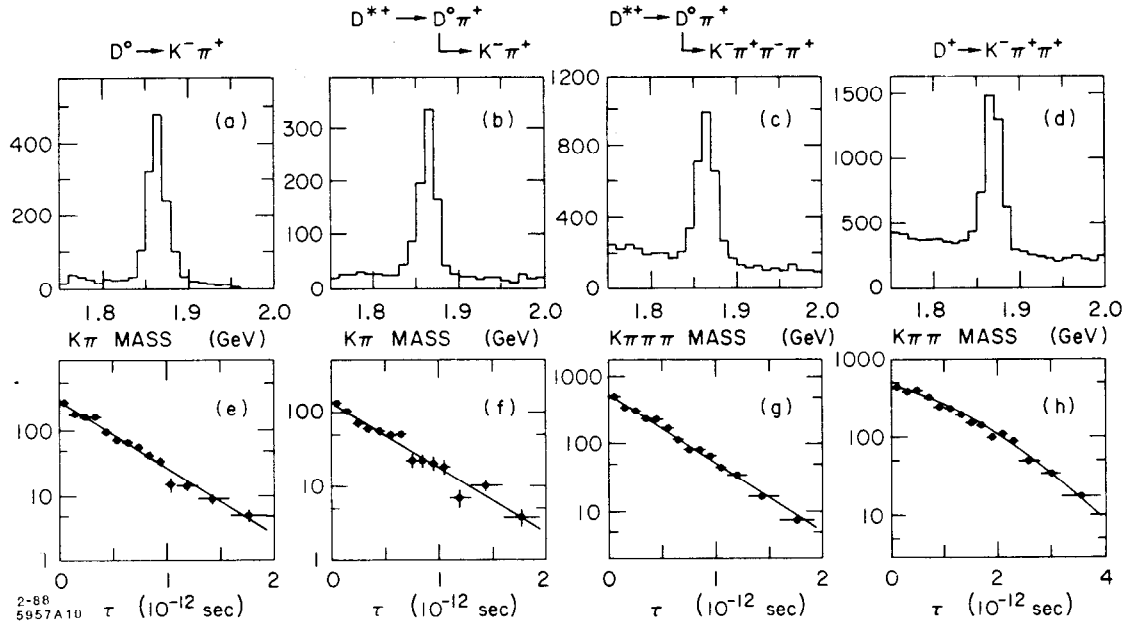

Fig. 12 E-691: Effective mass and decay time distributions for selected D decays.

Detailed studies have been performed to evaluate the effects of data selection and event reconstruction on the functions $f(t)$ and $b(t)$ and on the fitted lifetimes. The background subtraction affects the decay modes differently, the total effect on the average D^0 lifetime is a shift by $+0.030 \pm 0.002$ ps. The total acceptance correction amounts to -0.015 ± 0.005 ps. A global fit to all three subsamples gives

$$\tau(D^0) = 4.22 \pm 0.08 \pm 0.10 \cdot 10^{-13} \text{ s}.$$

The D^+ decay time distribution shows a clear deviation from the expected exponential; this is due to the limited length of the decay region and the longer average lifetime. The correction due to acceptance, resolution, and absorption in the target is -0.14 ± 0.02 ps, the background subtraction amounts to $+0.275 \pm 0.017$ ps. A fit to the data results in a lifetime of

$$\tau(D^+) = 10.9 \pm 0.3 \pm 0.25 \cdot 10^{-13} \text{ s}.$$

The charged D meson lifetime exceeds the lifetime of the neutral D meson by a factor of $2.58 \pm 0.09 \pm 0.08$.

The same data sample was used to study the D_s^+ lifetime. The D_s^+ mesons were identified by two different decay modes, $D_s^+ \to \phi\pi^+ \to K^-K^+\pi^+$ and $D_s^+ \to \overline{K}^{*o}K^+ \to K^-K^+\pi^+$. The mass spectra and corrected decay time distributions for the two sample are shown in Figure 13. There are two well separated mass peaks, one from the Cabibbo-suppressed decay of the D^+, the other from the decay of the

D_s^+. The decay time distributions include only decays in the mass region 1.953 – 1.985 GeV/c^2. The number of signal and background events are given in Table II. A maximum likelihood fit to the total sample of 228 D_s^+ decays gives a mean lifetime of

$$\tau(D_s^+) = 4.7 \pm 0.4 \pm 0.2 \cdot 10^{-13} \text{ s.}$$

The main contributions to the systematic error arise from the corrections for efficiency and resolution, –0.080 ± 0.017 ps, and from the background subtraction, +0.060 ± 0.015 ps. Decays $D^+ \to K^-\pi^+\pi^+$ and $\Lambda_c^+ \to pK^-\pi^+$ are estimated to contribute less than three background events to the total D_s^+ sample, however, their effect on the lifetime of the D_s^+ is small because they contribute roughly equally to signal and background.

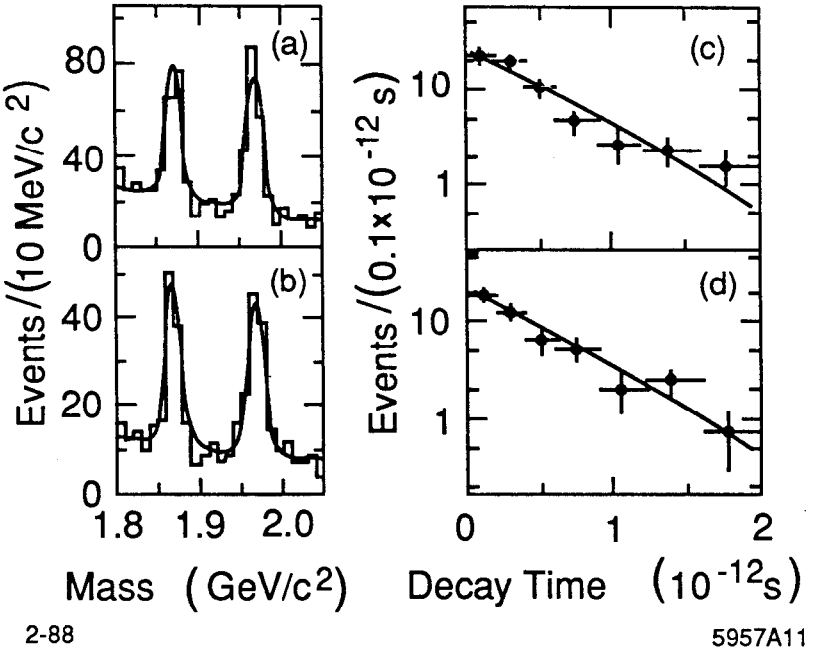

Fig. 13. E-691: Effective mass and decay time distribution for the decays $D_s^+ \to \phi\pi^+$ (a and c) and $D_s^+ \to \overline{K}^{*0}K^+$ (b and d).

Recently, the E-691 group[38] presented a measurement of the lifetime of the Λ_c^+ baryon. The analysis follows the same procedure outlined above for charm mesons. The results, based on the decay mode $\Lambda_c^+ \to pK^-\pi^+$, are given in Table II and in Figure 14. The background is substantially larger than for the charm meson decays, because of the smaller production cross section and the shorter lifetime. The systematic error, quoted as $\pm 0.2 \cdot 10^{-13}$ s, is dominated by the background subtraction and effects due to errors in the determination of the interaction vertex. The contamination from misidentified D^+ and D_s^+ decays is small.

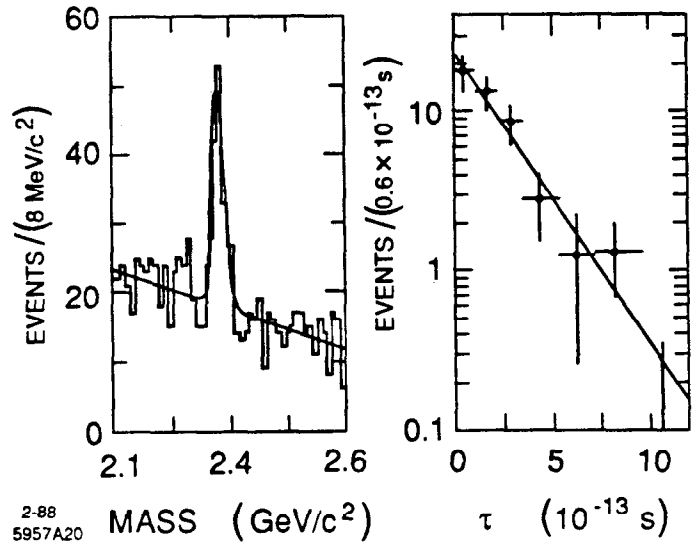

Fig. 14. E-691: Effective mass and decay time distribution for selected Λ_c^+ decays.

3.4 Wire Chambers

Among the ten $J^P = 1/2^+$ charm baryon states predicted by the standard SU_4 theory, only the lowest mass state, $\Lambda_c^+(\text{cud})$,* is well established at a mass of 2285.6 ± 1.8 MeV/c^2.[30] There are two fixed target experiments that have contributed lifetime measurements for charm baryons other than the Λ_c^+. Both experiments employ multi-wire proportional chambers with moderate resolution to enhance particle tracking close to the target.

3.4.1 CERN WA-62 The WA-62 collaboration was the first to present evidence for the strange charm baryons $\Xi_c^+(\text{csu})$ at a mass of 2460 ± 15 MeV/c^2[40] and $\Omega_c^0(\text{css})$ at 2740 ± 10 MeV/c^2.[41] The experiment was operated in the CERN hyperon beam with 135 GeV Σ^- on a beryllium target. The trigger was designed to select final states of strangeness s=−2 and s=−3 by requiring a K^- and a proton in the Cerenkov counters, and a V^0 decay in the spectrometer. The effective mass for the $\Lambda^0 K^- \pi^+ \pi^-$ combinations is shown in Figure 15a. There are 53 events in the peak above a background of 59 events. Even though the resolution in the longitudinal vertex position is only 6 mm, the experimenters are able to extract the lifetime from a simultaneous fit to pathlength distributions of the candidate events in the peak region and suitably normalized background events. The difference of these distributions shows a clear shift to positive decay lengths (Figure 15b). A fit yields

$$\tau(\Xi_c^+) = 4.8 \pm^{2.1}_{1.5} \pm^{2.0}_{1.0} \cdot 10^{-13} s.$$

The systematic error includes the uncertainties in the background and resolution

* The quark contents of the hyperon states is indicated to explain the nomenclature.

estimates and a possible shift due to charm mesons produced in association with the Ξ_c^+.

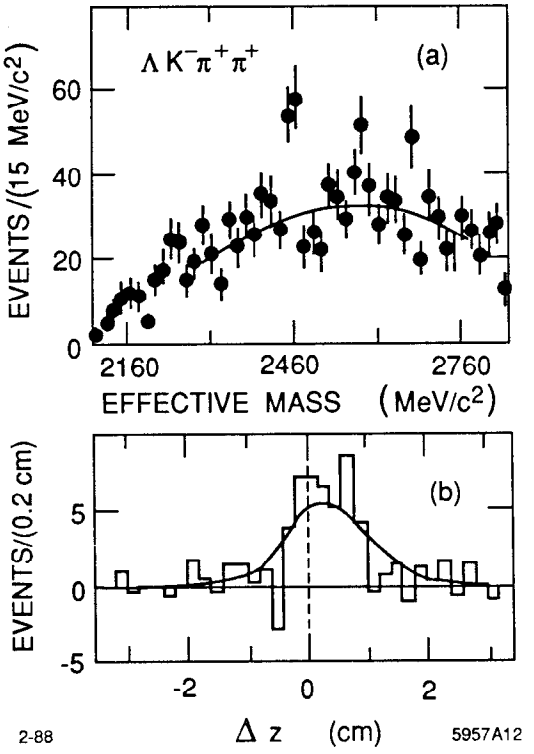

Fig 15. WA-62: Measurement of the lifetime of the Ξ_c^+ baryon, a) effective $\Lambda K^-\pi^+\pi^-$ mass for selected events, and b) background subtracted decay length distribution for the Ξ_c^+ signal.

The same experiment has searched for the production of the Ω_c^0 (css) baryon,[41] a state that decays weakly to final states of strangeness s=–3, like $\Xi^- K^-\pi^+\pi^+$. The data are presented in Figure 16. There are 20 decays $\Xi^- \rightarrow \Lambda^0\pi^-$ of which 6 have two additional tracks that are consistent with the decay $K^{*0}(896) \rightarrow K^-\pi^+$. Three of these six candidate decays cluster in a 30 MeV/c^2 wide interval of the effective mass of $\Xi^- K^-\pi^+\pi^+$. If one accepts these three decays as evidence for a Cabibbo-favoured decay of the charm baryon Ω_c^0, its mass is $2740 \pm 20 MeV/c^2$, and the mass difference of the two strange baryons is $M(\Omega_c^0) - M(\Xi_c^+) = 280 \pm 10 MeV/c^2$. From the reconstructed momentum and decay lengths of these candidates, one obtains the proper times 10.2 ± 4.2, 3.3 ± 5.6 and $8.5 \pm 5.3 \cdot 10^{-13}$ s. The average is

$$\tau(\Omega_c^0) = 7.9 \pm 2.8 \pm 2.0 \cdot 10^{-13} s.$$

3.4.2 FNAL E-400 The E-400 group at Fermilab presented a results on the production and lifetime of the Ξ_c^+ (csu) baryon.[42] The data were recorded in a high energy neutron beam by a large spectrometer with two magnets and three

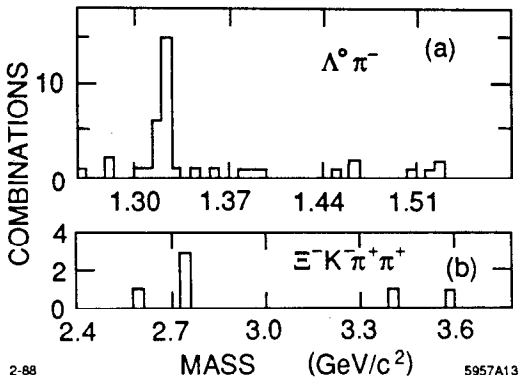

Fig. 16. WA-62: Evidence for the decay $\Omega_c^0 \rightarrow \Xi^- K^- \pi^+ \pi^-$ with $\Xi^- \rightarrow \Lambda^0 \pi^-$.

Cerenkov counters, placed downstream of a segmented target and a vertex detector of Silicon wafers and 9 planes of MWPC with 0.25 mm wire spacing. The resolution of the impact parameter was typically 60 μm, the average error on the longitudinal position of the interaction point was 1 mm. Figure 17 shows the $\Lambda^o K^- \pi^+ \pi^-$ effective mass for candidates for the decay of the Ξ_c^+ baryon. For these candidates, the $K\pi\pi$ vertex is required to be separated by 3σ from the primary vertex and the Λ^o momentum has to exceed the momentum of both pions and point back to the secondary vertex. The mass distribution shows two narrow peaks, separated by 72 ± 8 MeV/c^2. There are 32 ± 8 and 27 ± 11 events in two peaks. They are interpreted as two Cabibbo-favoured decays, $\Xi_c^+ \rightarrow \Lambda^o K^- \pi^+ \pi^-$ and $\Xi_c^+ \rightarrow \Sigma^o K^- \pi^+ \pi^-$. The separation of the two peaks corresponds to the energy of the missing photon from the decay $\Sigma^o \rightarrow \Lambda^o \gamma$. A maximum likelihood for a sum of a polynomial background and two Gaussian peaks yields a Ξ_c^+ mass of 2448 ± 5 MeV/c^2. The uncertainty of the absolute mass scale is estimated to be 30 MeV/c^2. The average lifetime for all decays was determined from a comparison of signal and background events with Monte Carlo simulations, the result,

$$\tau(\Xi_c^+) = 6.2 \pm^{1.8}_{1.6} \cdot 10^{-13} \text{ s},$$

agrees well with the earlier measurement by the CERN hyperon experiment.[40] However, the two experiments are not obviously compatible, as one would expect both to show the two peak structure in $M(\Lambda^0 K \pi \pi)$.

3.5 e^+e^- Experiments

A detailed discussion of the detectors that have been used to record data at the e^+e^- storage rings is presented elsewhere in this volume[43] and will not be repeated here. e^+e^- experiments have the advantage that 45% of the hadronic final states contain heavy flavour particles, and clean samples of charm particle decays can be obtained on the basis of kinematics alone, avoiding losses at short decay distances. The major disadvantage of colliding beam experiments is due to the fact that detectors have to be placed outside a beam pipe of several cm in radius.

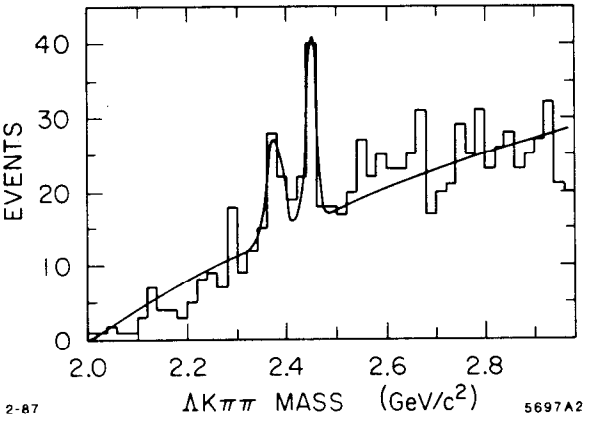

Fig. 17. E-400: Effective mass of candidates for the decays of the Ξ_c^+ baryon. The curve represents the result of a maximum likelihood fit taking into account the experimental resolution.

The DELCO group has published[44] a measurement of the D^0 lifetime based on the measurement of the impact parameter of the K^- and π^+ relative to the beam centre that is monitored by a set of four electrodes placed inside the vacuum chamber. A multi-cell Cerenkov counter and a very loose cut on the $D^{*+} - D^0$ mass difference are employed to select the decay modes $D^0 \to K^-\pi^+ +$ neutrals. The average impact parameter of 151.7 ± 42.5 μm translates to a lifetime $\tau(D^0) = 4.6 \pm 1.5 \pm^{0.7}_{0.6} \cdot 10^{-13}$ s. Systematic studies show that the measurement is largely bias free and insensitive to small errors in alignment or resolution.

The Mark II collaboration[45] was the first of the e^+e^- experiments to published measurements of the D^0 and D^+ lifetimes. Since then the HRS,[47,48] TASSO,[49,50] CLEO,[51] and ARGUS[52] groups have presented results on D^0, D^+, and D_s^+ lifetimes. Since space is limited and the analyses are very similar for these experiments, only the CLEO analysis will be described in detail.

The CLEO analysis relies primarily on the good spatial resolution of the two cylindrical drift chambers, a 10 layer vertex chamber with a 85 μm resolution and a larger volume chamber with 17 layers and 160 μm resolution. The vertex detector is a drift chamber with a hexagonal array of sense and field wires, the innermost layer is located 8.5cm from the beam axis. The chambers are operated in a 10 kGauss magnetic field and are instrumented to measure drift time and specific ionization. The longitudinal position is measured by charge division on the 70 cm long sense wires in the vertex chamber, and by cathode strips on the inner and outer shells of the tracking volume. At the interaction point, the extrapolation error for a single high momentum track is approximately 100 μm. Candidates for the following charm meson decay modes are selected (a) $D^{*+} \to D^0\pi^+$, $D^0 \to K^-\pi^+$, (b) $D^+ \to K^-\pi^+\pi^+$, and (c) $D_s^+ \to \Phi\pi^+$, $\Phi \to K^-K^+$. The kaons are identified by time-of-flight measurements or by dE/dx in the drift chamber gas. Appropriate mass cuts are applied to select the D^{*+} and Φ decays. Additional cuts on the particle

momenta and angles further enhance the signals. The decay point of a charm meson candidate is determined as the fitted intersection of all charged secondaries. The fitting procedure incorporates the uncertainties due to multiple scattering, spatial resolution and track finding, and only vertices with χ^2/dof less than 6 are retained. Given the limited resolution, it is not possible to measure the beam interaction point on an event by event basis. For this reason, the size and average position of the beam interaction region in the plane transverse to the beam direction is determined on a run-by-run basis from the measured distribution of the vertices in hadronic events. This procedure yields the beam centre to an accuracy of 20 μm in the vertical and 40 μm in the horizontal direction. The corresponding measured widths of the beams are 150 μm and 1200 μm, respectively.

The decay length for each charm candidate is determined by measuring the most probable path length in the transverse plane,

$$l_{xy} = \frac{xt_xB_{xx} + yt_yB_{yy} + B_{xy}(t_xy + t_yx)}{t_x^2B_{xx} + t_y^2B_{yy} + 2t_xt_yB_{xy}},$$

where x and y are the fitted coordinates of the decay vertex relative to the beam center, t_x and t_y are the direction cosines of the candidate's transverse momentum. B is the inverse of the error matrix, combining errors from both the decay vertex and the beam position. Thus the error on the transverse decay length is

$$\sigma_{xy} = \sqrt{B_{yy}t_x^2 + B_{xx}t_y^2 + 2B_{xy}t_xt_y}.$$

The proper decay length and error are then

$$l = ct = \frac{l_{xy}}{\beta\gamma sin\theta} \quad \text{and} \quad \sigma_l = \frac{\sigma_{xy}}{\beta\gamma sin\theta},$$

where θ is the polar angle of the decaying particle with respect to the beam axis.

In Figure 18 the distributions in effective mass and decay distance are shown for the three decay modes measured by the CLEO collaboration. There are 247 D^0, 317 D^+ and 87 D_s^+ decays above backgrounds of 28, 279, and 54, respectively. Although the measurement of the decay distances is seriously limited by the detector resolution and the beam size, the displacement of the nearly Gaussian distributions to positive values is apparent. The observed distributions are fitted to a sum of two contributions, the charm particle decay distribution $s(l)$ and the background distribution $b(l)$, represented by

$$L(l) = (1 - f_b)\ s(l) + f_b\ b(l).$$

The density functions $s(l)$ and $b(l)$ are of the form

$$s(l) = \frac{1}{\sqrt{2\pi}\sigma_l\lambda} \int_0^\infty d\xi\ e^{-l/\lambda}\ e^{(l-\xi)^2/\sigma_l^2},$$

where the exponential decay distribution is folded with a Gaussian resolution func-

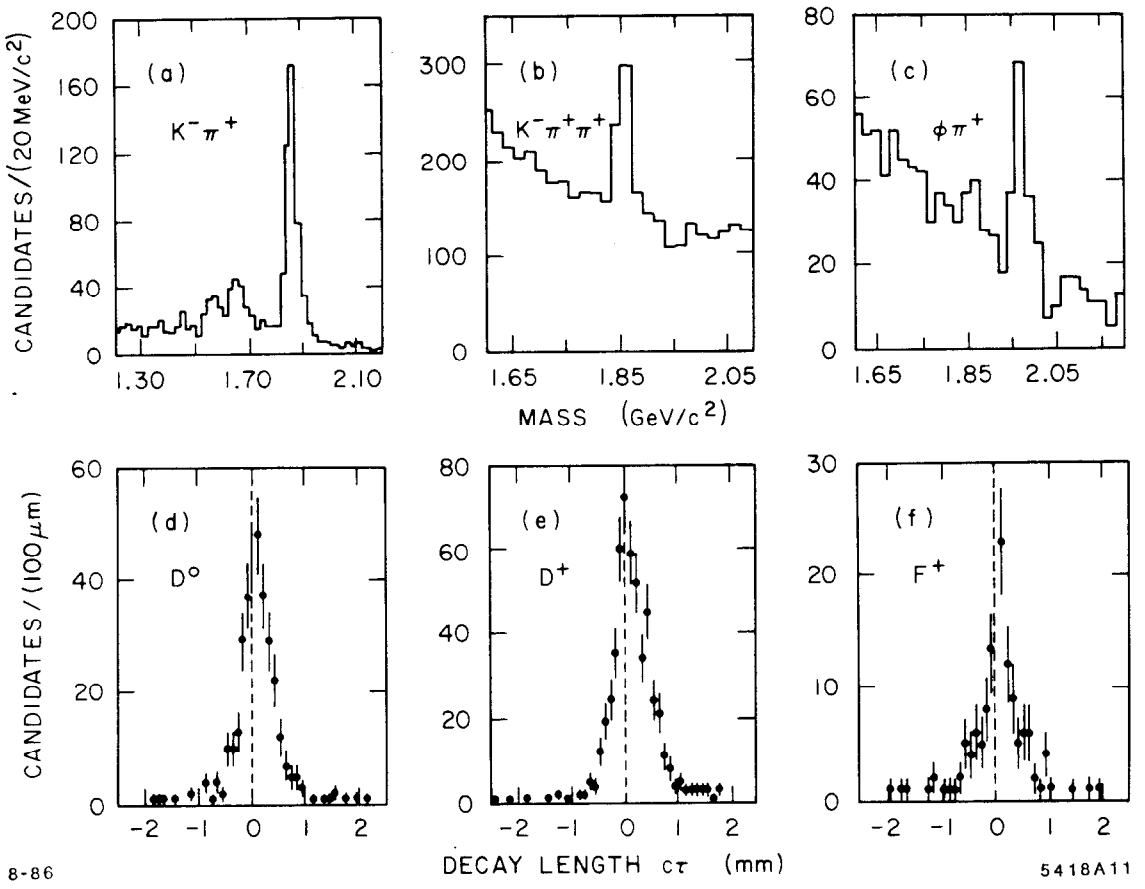

Fig. 18. CLEO: Effective mass and decay length distributions for D^0, D^+, and D_s^+ decays.

tion of width σ_l. The background is measured separately for decays that pass all the selection criteria except for having an invariant mass outside the signal region. The background proper decay lengths are measured to be small, but not zero, due to tracks from charm and strange particle decays. The normalisation of the background, f_b, is obtained from a fit to the invariant mass distribution using a Gaussian signal on top of a polynomial background. Maximum likelihood fits to the proper decay length distributions in Figure 18 give average decay lengths of 138 ± 19 μm, 173 ± 20 μm, and 93 ± 37 μm for the D^0, D^+, and D_s^+ decay modes, respectively. The corresponding background distributions are measured to give 14 ± 39 μm, 22 ± 8 μm, and 19 ± 38 μm. These fitted decay lengths translate to the following lifetimes

$$\tau(D^0) = 5.0 \pm 0.7 \pm 0.4 \cdot 10^{-13}\ s, \quad \tau(D^+) = 11.4 \pm 1.6 \pm 1.0 \cdot 10^{-13}\ s,$$

and

$$\tau(D_s^+) = 4.6 \pm 2.1 \pm 0.5 \cdot 10^{-13}\ s.$$

The systematic errors include the uncertainties in the detector resolution, effects

of track and vertex fitting methods, the background subtraction, and the beam position. The lifetime ratios are

$$\tau(D^+)/\tau(D^0) = 2.3 \pm 0.5 \qquad \text{and} \qquad \tau(D_s^+)/\tau(D^0) = 0.9 \pm 0.5.$$

2.5 Summary on Charm Particle Lifetimes

An enormous effort has gone into the measurement of charm particle lifetimes, in both fixed target and e^+e^- experiments. A compilation of the presently available results is given in Tables III and IV.

Table III: Measurements of Lifetimes of Charmed Mesons

		D^+		D^o		D_s^+	
Experiment	Ref.	Decays	$\tau(10^{-13}$ s)	Decays	$\tau(10^{-13}$ s)	Decays	$\tau(10^{-13}$ s)
E-531	9	23	$11.1\pm^{4.4}_{2.9}$	58	$4.3\pm^{0.7}_{0.5}\pm^{0.1}_{0.2}$	6	$2.6\pm^{1.6}_{1.1}$
WA-58	10	27	$5.0\pm^{1.5}_{1.0}\pm1.9$	44	$3.6\pm^{1.2}_{0.8}\pm0.7$		
SHF	11	48	$8.6\pm1.3\pm^{0.7}_{0.3}$	50	$6.1\pm0.9\pm0.3$		
NA-16	12	15	$8.4\pm^{3.5}_{2.2}$	16	$4.1\pm^{1.3}_{1.0}$		
NA-18	13	7	$6.3\pm^{4.9}_{2.3}\pm1.5$	9	$4.1\pm^{2.6}_{1.3}\pm0.5$		
NA-27	14	149	$11.2\pm^{1.4}_{1.1}$	145	$4.6\pm^{0.6}_{0.5}$		
NA-1	25,26	98	$9.5\pm^{3.1}_{1.9}$	51	$3.4\pm^{0.6}_{0.5}$		
NA-14	28			173	4.43 ± 0.37		
NA-11	30	28	$10.6\pm^{3.6}_{2.4}\pm1.6$	26	$3.7\pm^{1.0}_{0.7}\pm0.5$	9	$3.2\pm^{1.5}_{1.0}$
	31	69	$11.2\pm^{1.6}_{1.3}\pm0.8$				
NA-32	32,33	59	$10.9\pm^{1.9}_{1.5}$	92	4.2 ± 0.5	12	$3.4\pm^{1.3}_{0.9}$
NA-32+	33					16	$4.5\pm^{1.9}_{1.1}$
E-691	37	4212	$10.9\pm0.5\pm0.25$	2992	$4.22\pm0.08\pm0.10$	228	$4.7\pm0.4\pm0.2$
DELCO	44				$4.6\pm1.5\pm^{0.7}_{0.6}$		
MKII	45	16	$8.9\pm^{3.8}_{2.7}\pm1.3$	66	$4.7\pm^{0.9}_{0.8}\pm0.5$		
MKII+	46			53	$4.4\pm^{1.2}_{1.1}\pm0.6$		
HRS	47,48	114	$8.1\pm1.2\pm1.6$	53	$4.2\pm0.9\pm0.6$	13	$3.5\pm^{2.4}_{1.8}\pm0.9$
TASSO	49,50			48	$4.8\pm^{1.0}_{0.9}\pm^{0.5}_{0.7}$	9	$5.7\pm^{3.6}_{2.6}\pm0.9$
CLEO	51	247	$11.4\pm1.6\pm0.7$	317	$5.0\pm0.7\pm0.4$	87	$4.6\pm2.2\pm0.5$
ARGUS	52	363	$10.5\pm0.8\pm0.7$	776	$4.8\pm0.4\pm0.3$	114	$5.6\pm^{1.3}_{1.2}\pm0.8$
Total		5475	$10.69\pm^{0.32}_{0.30}$	4969	4.33 ± 0.10	494	$4.57\pm^{0.38}_{0.33}$

In an attempt to combine the available information, averages and combined errors have been calculated. All individual results, whether final or preliminary, have been weighted by the inverse square of the fractional error, a recipe that in the limit of perfect resolution and negligible acceptance corrections corresponds to

the number of events in the sample, which is the correct weight for an exponential distribution. (For large Gaussian errors like in e^+e^- experiments, however, the inverse square of the total error is the more appropriate weight.) Using the combined statistical and systematic errors quoted, the best estimate for the lifetime of the charmed mesons are, in units of 10^{-13} s,

$$\tau(D^0) = 4.33 \pm 0.10\ , \qquad \tau(D^+) = 10.7 \pm 0.3\ , \qquad \tau(D_s^+) = 4.6 \pm^{0.4}_{0.3}\ .$$

The lifetimes of the charged and neutral D mesons are clearly different, the average of the ratio measured by individual experiments is

$$\tau(D^+)/\tau(D^0) = 2.40 \pm 0.10.$$

A comparison of the lifetimes and semi-leptonic branching ratios of D^0 and D^+ provides the first clue as to the origin of this difference. The Mark III group[53] has reported separate semi-leptonic branching ratios, $BR(D^+ \to e^+X) = 0.170 \pm 0.019 \pm 0.007$, and $BR(D^0 \to e^+X) = 0.075 \pm 0.011 \pm 0.004$. The ratio

$$BR(D^+ \to e^+X)/BR(D^0 \to e^+X) = 2.3 \pm^{0.5}_{0.4} \pm 0.1,$$

is in agreement with the lifetime ratio. Since the purely leptonic widths of the charm mesons are negligible and the semi-leptonic partial widths of the D^0 and D^+ should be nearly equal (unless Cabibbo-suppressed processes play a major role in D^+ decay), a difference in the lifetime and semi-leptonic branching ratios implies a difference in the hadronic widths of the two states.

Measurements of the D_s^+ lifetime have in the past suffered from extremely low statistics and the contamination from D^+ and Λ_c^+ decays. New data from the fixed target experiments E-691 and NA-32 and the e^+e^- storage ring experiments, CLEO and ARGUS, show that the D_s^+ and D^+ lifetimes are comparable,

$$\tau(D_s^+)/\tau(D^0) = 1.11 \pm 0.10.$$

Among the four charmed baryons which are expected to decay by weak interactions, only the lowest mass state, Λ_c^+, is well established. Data for the strange charm baryons, Ξ_c^+ and Ω_c^0, are still very scarce, the Ξ_c^0 has not yet been found. There exists only one measurement of the Λ_c^+ semi-leptonic branching ratio,[54] $BR(\Lambda_c^+ \to e^+X) = 0.045 \pm 0.017$, which, together with the short Λ_c^+ lifetime, points to a substantial non-leptonic enhancement in the decay.

While the naive spectator model[55] correctly predicts the order of magnitude of charm particle lifetimes, it fails to account for the observed differences,

$$\tau(D^+) > \tau(D^0) \simeq \tau(D_s^+) \quad \text{and} \quad \tau(\Lambda_c^+) < \tau(\Xi_c^+) \simeq \tau(\Omega_c^0).$$

Table IV: Measurements of Lifetimes of Charmed Baryons

Experiment	Ref.	Λ_c^+ Decays	Λ_c^+ $\tau(10^{-13}$ s)	Ξ_c^+ Decays	Ξ_c^+ $\tau(10^{-13}$ s)	Ω_c^o Decays	Ω_c^o $\tau(10^{-13}$ s)
E-531	9	13	$2.0\pm^{0.7}_{0.6}$				
WA-58	10	11	$2.3\pm^{0.9}_{0.6}\pm0.4$				
NA-27	16	9	$1.2\pm^{0.5}_{0.3}$				
NA-1	27	9	$1.1\pm^{0.8}_{0.4}$				
NA-32	34,35	37	$1.6\pm^{0.4}_{0.3}\pm0.3$				
E-691	38	97	$2.2\pm0.3\pm0.2$				
WA-62	40,41			53	$4.8\pm^{2.1}_{1.5}\pm^{2.0}_{1.0}$	3	$7.9 \pm 2.8 \pm 2.0$
E-400	42			59	$6.2\pm^{1.8}_{1.6}$		
Total		176	1.9 ± 0.2	112	$5.7 \pm^{1.6}_{1.2}$	3	7.9 ± 3.4

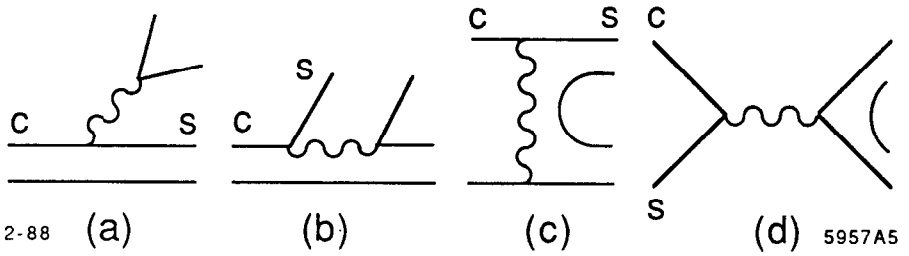

Fig. 19. Quark diagrams representing hadronic decays of charm mesons: a,b) spectator diagrams common to D^0 and D^+, c) W^+ exchange, and d) annihilation for D_s^+.

Two main mechanisms have been suggested to account for these differences, light quark interference[56] and W-exchange or annihilation.[57,58] These basic processes are illustrated in Figure 19, a detailed discussion is given in the article on charm particle decay in this volume.[2] The interference mechanism is based on the fact that the final state resulting from D^+ decay contains two $\bar{d}$ quarks, one is the light constituent of the D^+, the other emerges from the decay of the charm quark, $c \rightarrow s\bar{u}\bar{d}$. The interference of these identical quarks is destructive due to the Pauli principle, it suppresses the D^+ decays with respect to D^0. On the other hand, the W-exchange process $c\bar{u} \rightarrow s\bar{d}$ and the W-annihilation $c\bar{s} \rightarrow u\bar{d}$ are only operative in D^0 and D_s^+ decay, shortening their lifetimes relative to D^+. In contrast to the spectator decay, both of these effects are controlled by the quark wave functions, which are a priori not well known. Straightforward quark model estimates[59] indicate a sizable interference effect, but give negligible contributions from W-exchange and annihilation due to helicity and colour suppression at the light quark vertex. It has been suggested that soft gluon radiation may lift such constraints,[58] however,

quantitative estimates of such effects are very difficult to obtain. It has also been proposed that short distance QCD corrections could give a sizable non-leptonic enhancement and decrease the semi-leptonic branching ratios. This would be equal for D^0 and D^+, unless the enhancement was cancelled by the interference effect in D^+ decays.[60] It has become an accepted procedure to keep only the leading contribution in the expansion of the non-leptonic decay rates in powers of $1/N_c$, N_c being the number of colour degrees of freedom. This procedure is suggested by theoretical consistency arguments and by an analysis of two-body hadronic decays. The net effect is a major improvement in the agreement between theory and experiment, both in exclusive and inclusive decay rates.[61,62] It is also uncertain how strongly final state interactions influence decay rates. The observation of a relatively large branching ratio[63–65] for the decay $D^0 \to \Phi\overline{K^0}$ may indicate that they play an important role.[66]

Interference of quarks and W-exchange are also expected to be important for charm baryon decay and to give rise to different lifetimes. (Annihilation to a virtual W is not possible because of the absence of antiquarks.) The essential difference to charm mesons lies in the fact that W-exchange among valence quarks of baryons is neither helicity nor colour suppressed, in fact, they are expected to dominate Λ_c^+ decay. More specifically, W-exchange does not depend on soft gluon radiation which is difficult to calculate. Depending on the quark contents of the weakly decaying charm baryons, Λ_c^+, Ξ_c^+, Ξ_c^0, and Ω_c^0, the non-spectator effects contribute differently to hadronic widths and thus generate different lifetimes. Specific predictions have been made and are judged to be reliable,[67,68]

$$\tau(\Omega_c^0) \;:\; \tau(\Xi_c^0) \;:\; \tau(\Lambda_c^+) \;:\; \tau(\Xi_c^+) \;\simeq\; 0.6 \;:\; 0.6 \;:\; 1.0 \;:\; 1.6.$$

Obviously, much better data are needed to challenge these predictions.

In summary, lifetime measurements of charm mesons have substantially improved in recent years. Though the lifetime differences can be qualitatively understood in terms of quark interference and gluon enhanced W-exchange, quantitative predictions remain difficult. In response to large amounts of data on exclusive decays, comprehensive phenomenological analyses[61] [62] of two-body hadronic decays have been performed and have substantially improved our understanding of charm meson decay. It is expected that more precise measurements of the decay modes, in particular of the D_s^+ and charm baryons, will further enhance our understanding of heavy flavour decays.

4. Lifetimes of Beauty Particles

With the exception of a single *beautiful* event observed in an emulsion at CERN[69] all our information on the lifetime of beauty particle comes from experiments at the e^+e^- storage rings PEP and PETRA. It has been five years since the MAC[70] and

Mark II[71] collaborations first reported B lifetimes in the range of 10^{-12} sec, substantially longer than anticipated. These first measurements have been confirmed by other experiments at PEP and PETRA, and now updates of earlier results with additional data, improved detectors and refinements in the analysis are available.

The experiments at PEP and PETRA have many things in common. They all have cylindrical symmetry relative to the beam pipe. The central section is designed to measure charged particle tracks, the outer sections provide lepton identification and calorimetry. All detectors use a cylindrical drift chamber with wires parallel to or at small angles to the beam axis. The tracking volume is embedded in the field of a solenoid magnet. Because of this particular choice of geometry, the space resolution is much better in the plane perpendicular to the beam. All experiments have improved the accuracy of the charged particle tracking by the installation of a small, high precision drift chamber mounted on the outside of the thin walled beam pipe. In general, the detection efficiency and the resolution for neutral particles, like π^0 and η^o, is much inferior to charged particles, and they are not used in the analysis.

The e^+e^- interaction point at which the B particles are produced is located somewhere inside the interaction region of the two beams. The size and center of this region is measured using tracks in Bhabha or hadronic events averaged over extended periods of time. Typically the interaction region is 400 μm wide horizontally and 50-70 μm wide vertically, it extends several cm longitudinally.

At c.m. energies of 15 GeV and above, 1/11 of all multi-hadron events contain pairs of beauty particles, mostly mesons. At these energies, the final state hadrons are produced in jet-like formations, with limited transverse momenta relative to the axis of the jets. Most events have two back-to-back jets due to fragmentation of the produced $q\bar{q}$ pair. The emission of hard gluons adds more jet-like fragments. Two-jet events can be divided into two separate jets by a plane perpendicular to the sphericity or thrust axis in such a way that each jet contains primarily the fragments and decay products from one of the initial quarks. In $b\bar{b}$ events, the total charged particle multiplicity is $n_b = 16 \pm 0.5 \pm 1.0$, there are on the average 5.2 charged particles produced in addition to the pair of beauty particles.

Due to the weak decay chain $b \rightarrow c \rightarrow s$, events containing B hadrons are of quite complicated topology. They have four vertices in addition to the production vertex, namely one for each beauty particle and one for each charm particle. In B meson decay, the average charged particle multiplicity is 3.8 ± 0.4 and 6.0 ± 0.3 for semi-leptonic and hadronic decays, respectively. These numbers include particles from the secondary charm decay. Given the complexity of these events and the small branching ratios for any exclusive decay mode, it is not surprising that experimenters cannot rely on fully reconstructed B decays to select B particle decays and measure the associated decay time.

In spite of the many similarities among experiments, there are substantial differences not only in the detector performances, but primarily in the details of the

data analysis. The two major challenges in the measurements of the B lifetime are a) the selection of events containing B hadrons, and b) the extraction of an estimate for the average decay time.

4.1 Selection of Events containing Beauty Particles

All of the experiments at PEP have relied on leptons with large transverse momentum to tag events containing B decays. This method is based on the well understood dynamics of semi-leptonic decays. The average transverse momentum of leptons from semi-leptonic decays of heavy flavour particles scales with the quark mass. Hence, beauty decays can be distinguished from charm decay and hadrons from background events because of the high mass of the b quark. The transverse momenta are measured relative to the jet axis which approximates the direction of the heavy quark rather well.

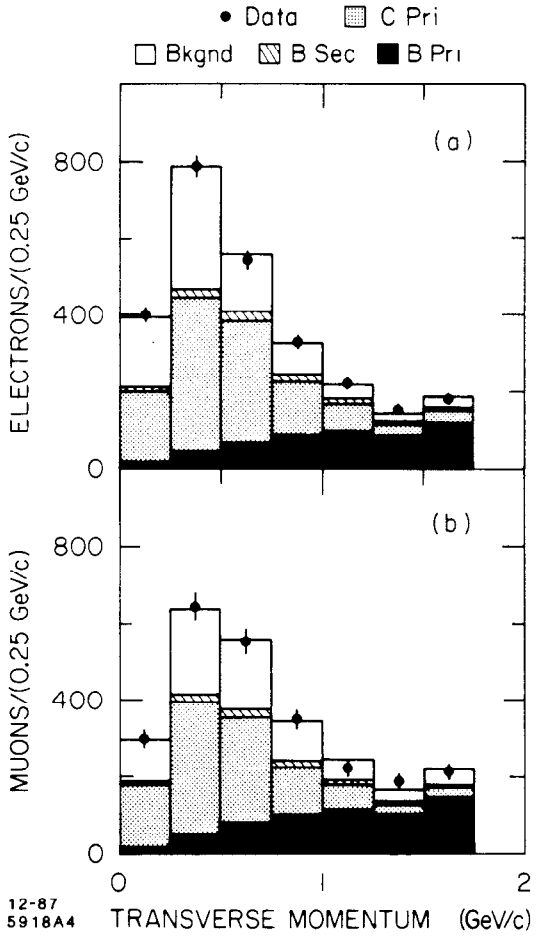

Fig. 20. Mark II: Transverse momentum spectra for a) 2631 electrons and b) 1230 muons with momenta greater than 2 GeV/c. The various contributions to the spectra are determined by a fit to the data.

All of the PEP experiments have measured inclusive lepton production as a function of the lepton momentum and its component transverse to the jet axis. Experiments differ in their methods of lepton identification, and obtain different degrees of purity of their sample of beauty events.[72-74] As an example, we show the most recent analysis reported by the Mark II group.[75] The authors have performed a fit to the entire lepton (p, p_t) spectrum in terms of contributions from beauty decay, charm decay, and background. The fit determines the average semi-leptonic branching ratios and the average energy of the charm and beauty particles in the sample. The total $b\bar{b}$ and $c\bar{c}$ production is presumed known. The measurement of the branching ratios provides a consistency check with other experiments. The measured transverse momentum spectra are shown in Figure 20. Leptons with p_t greater than 1 GeV/c originate to $(65 \pm 5)\%$ from B decay. This sample of B decays can be isolated with an efficiency of 7.5%. This method of tagging B events has the advantage that the B contents of the sample is derived from the data, based on well known transverse momentum spectra for semi-leptonic decays. Also, the average energy of the B hadron is extracted from the data, $< z >= 0.83 \pm 0.07$. The knowledge of the B fragmentation is important for the lifetime measurement, because the B particle momentum is not known for individual decays.

Experiments at PETRA have chosen a different method to select events containing beauty decays. It is based on the observation that $b\bar{b}$ events are more spherical than events resulting from the fragmentation of lighter quarks. In this method, each event is divided into two halves by a plane perpendicular to the sphericity axis. For each half, the observed particles are boosted into a frame that approximates the rest frame of a hypothetical B meson, moving with $\beta = 0.74$ along the sphericity axis. The purpose of this boost is to differentiate between $b\bar{b}$ events with large sphericity and events from charm and light quark fragmentation. The sphericity for each event half is calculated in its boosted frame. A comparison of the product of the two sphericities $s_1 \times s_2$ for $b\bar{b}$ events and lighter quark events is shown in Figure 21. Also given are the efficiency for selecting $b\bar{b}$ events and the purity of the sample as a function of a cut excluding events below a given value of $s_1 \times s_2$. The advantage of selecting B events on the basis of this boosted sphericity is the relatively high efficiency. However, the $b\bar{b}$ contents of the sample and the B hadron momentum have to be derived from a Monte Carlo simulation of the quark fragmentation, and this contributes a substantial systematic uncertainty.

4.2 Impact Parameter Measurements

Up to now only very few exclusive B decays have been observed at energies well above the threshold region. This is due to the small branching ratios and low detection efficiency. Consequently, the experiments have resorted to other less conventional methods of estimating the beauty lifetime. None of these methods distinguishes between different beauty mesons or baryons, but rather results in a measurement of the average lifetime of the detected beauty decays in the selected sample. The PEP experiments DELCO, MAC, Mark II, and HRS measure impact

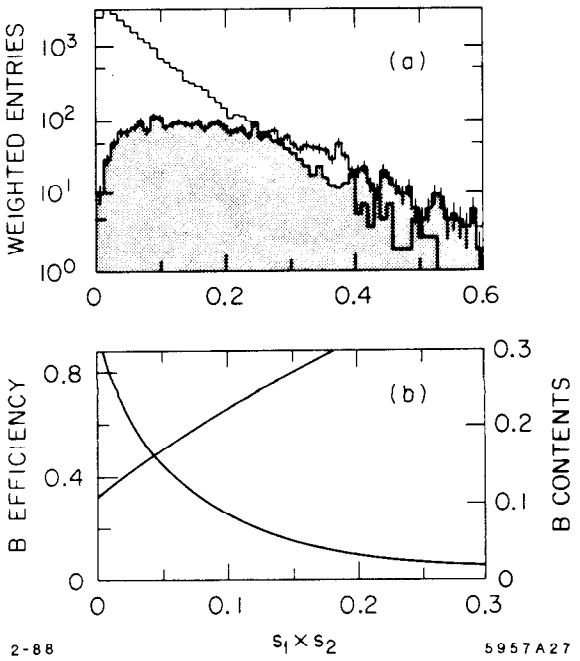

Fig. 21. JADE: A Monte Carlo simulation of the boosted sphericity product, a) distribution of $b\bar{b}$ events (dotted) and all hadronic events, and b) the detection efficiency and fraction of B events as a function of a cut imposed on $s_1 \times s_2$.

parameters of individual tracks in events selected by high leptons, while JADE and TASSO obtain a measure of the B lifetime from the position of the average vertex of tracks in a jet. The various techniques are illustrated in Figure 22.

All of the PEP experiments tag candidates for $b\bar{b}$ events by selecting high p_t leptons and then determine a signed impact parameter, δ, in the plane transverse to the beam direction. The impact parameter is defined as the projected distance of closest approach from the assumed B production point. δ is positive if the intersection point of the lepton trajectory with the assumed B trajectory corresponds to a positive decay length, it is negative otherwise. The impact parameter δ is related to the B decay length l by

$$\delta = l \cdot sin\theta \; sin\psi,$$

where θ is the polar angle of the B momentum and ψ the angle between the lepton trajectory and the B momentum. At the c.m. energy of 29 GeV, the average decay length of B hadrons is $\approx$ 600 μm for a B lifetime of 1 ps. The average impact parameter is 145 μm. There is a trivial correlation between the decay angle ψ and the B momentum. As the momentum ($p = \beta\gamma m$) increases the angle ψ decreases. As a result, the impact parameter becomes independent of momentum for large values of $\beta\gamma$. At PEP energies, where $\beta\gamma \approx$1.9, the average impact parameter still depends weakly on the B momentum, but this dependence is considerably weaker than the

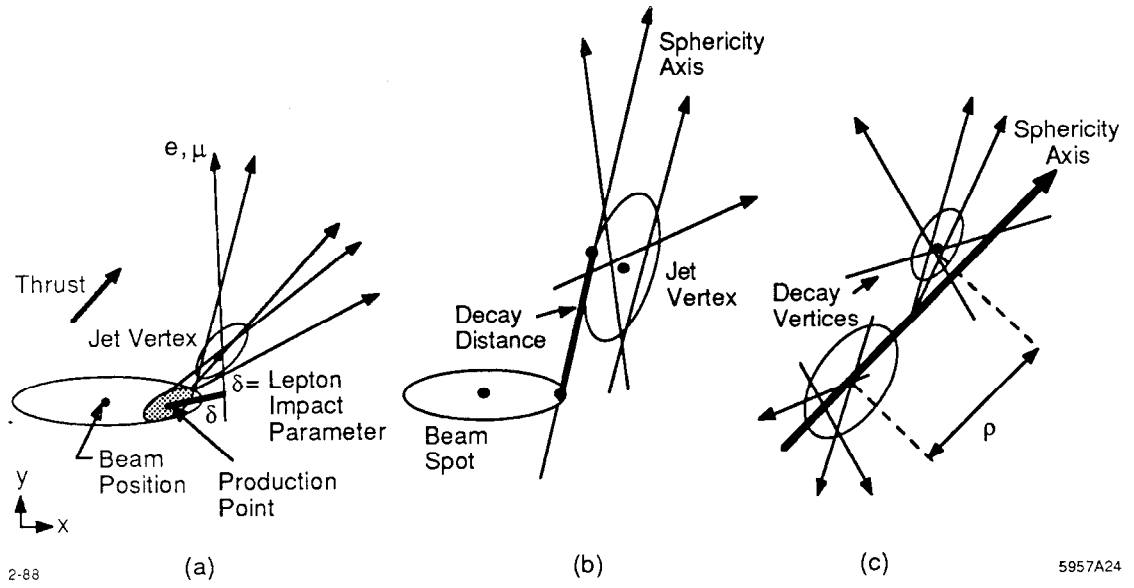

Fig. 22. Definition of the a) impact parameter, δ, b) the decay length, l, and c) the dipole length, ρ, in the plane transverse to the direction of the colliding beams.

dependence of the decay length on the $\beta\gamma$. Consequently, the determination of the lifetime from the impact parameter distribution is less sensitive to the uncertainties in the B momentum than a derivation based on a decay length distribution.

The impact parameter is a strong function of the lepton momentum component transverse to the B direction. To select semi-leptonic B decays, only leptons with high p_t, typically $> 1GeV/c$, are used. Conveniently, the impact parameters for these tracks are sizable (Figure 23b).

The error on the impact parameter measurement has several contributions, and these are illustrated in Figure 23a. In the limit of perfect resolution, the lepton impact parameters are positive, and one expects an exponential distribution. Since the B hadrons are not fully reconstructed, their direction is not known. Instead, the thrust axis is used to approximate the B direction. This is an approximation because of tracking losses and undetected neutral particles; the uncertainty is of the order of 0.15 rad. As a result of this error, the impact parameter distribution is slightly shifted to lower values. There are two dominant contributions to the error on the impact parameter. The first is due to the error in the extrapolation of the lepton trajectory measured in the vertex tracking chamber, this is typically $50-120\,\mu$m, depending on the position resolution of the vertex detector, its distance from the beam, and the amount of multiple scattering in the beam pipe and the chamber walls. The second, more important contribution is due to the uncertainty in the B production point. To first order, the measured center of the beam can serve as an unbiased estimate of the interaction point. This introduces errors given by

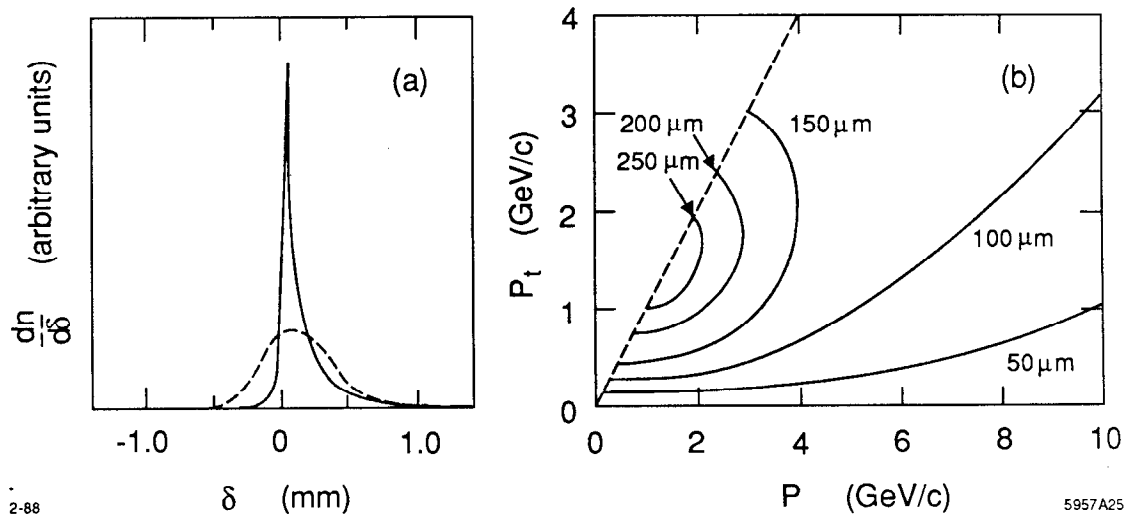

Fig. 23. Impact parameter distribution for leptons from B decay, a) including the effects of uncertainties in the thrust direction (solid line) and including the uncertainty in the B production vertex (dashed line), and b) the average impact parameter as a function of total and transverse momentum of the leptons.[76]

the horizontal and vertical size of the beam envelope. It is clearly advantageous to determine the B production point with better precision, on an event by event basis. It has been demonstrated that a secondary vertex formed by all tracks in a jet lies on the line connecting the production and decay point of the B particle. This is somewhat surprising, since the only track known to originate from the B decay is the high p_t lepton. Thus, one can determine the B production point by extrapolating from the jet vertex along the jet axis into the beam ellipse. To avoid biases, usually only well measured, high momentum tracks are included in the determination of the jet vertex. Also, particular care has to be taken so as not to reject vertex fits for events that contain long-lived hadrons with multiple vertices. Also, there are two estimates for the production vertex per event, one from each of the two jets, and a check can be made to make sure that they agree.

The B lifetime is determined from the measured impact parameter distributions. Results from the four PEP experiments are shown in Figure 24. The requirement to detect a high p_t lepton reduces the statistical power of the impact parameter method relative to other measurements. Nevertheless, there are a number of advantages in terms of smaller systematic errors. The impact parameter is inherently less sensitive to the B momentum. The impact parameter technique is also less sensitive to the charm lifetime and fragmentation. In general, the measurement relies much less on the Monte Carlo simulation to reproduce the characteristic properties of the event, like charged particle multiplicities and angles.

4.2.1 MAC The MAC collaboration[77] has published an analysis based on 100,000 multi-hadron events collected at PEP, 30% of which were recorded with a high resolution vertex detector. This device was installed on the outside of a vacuum pipe of 3.5 cm radius. It consisted of 6 layers of thin-walled tubes counters

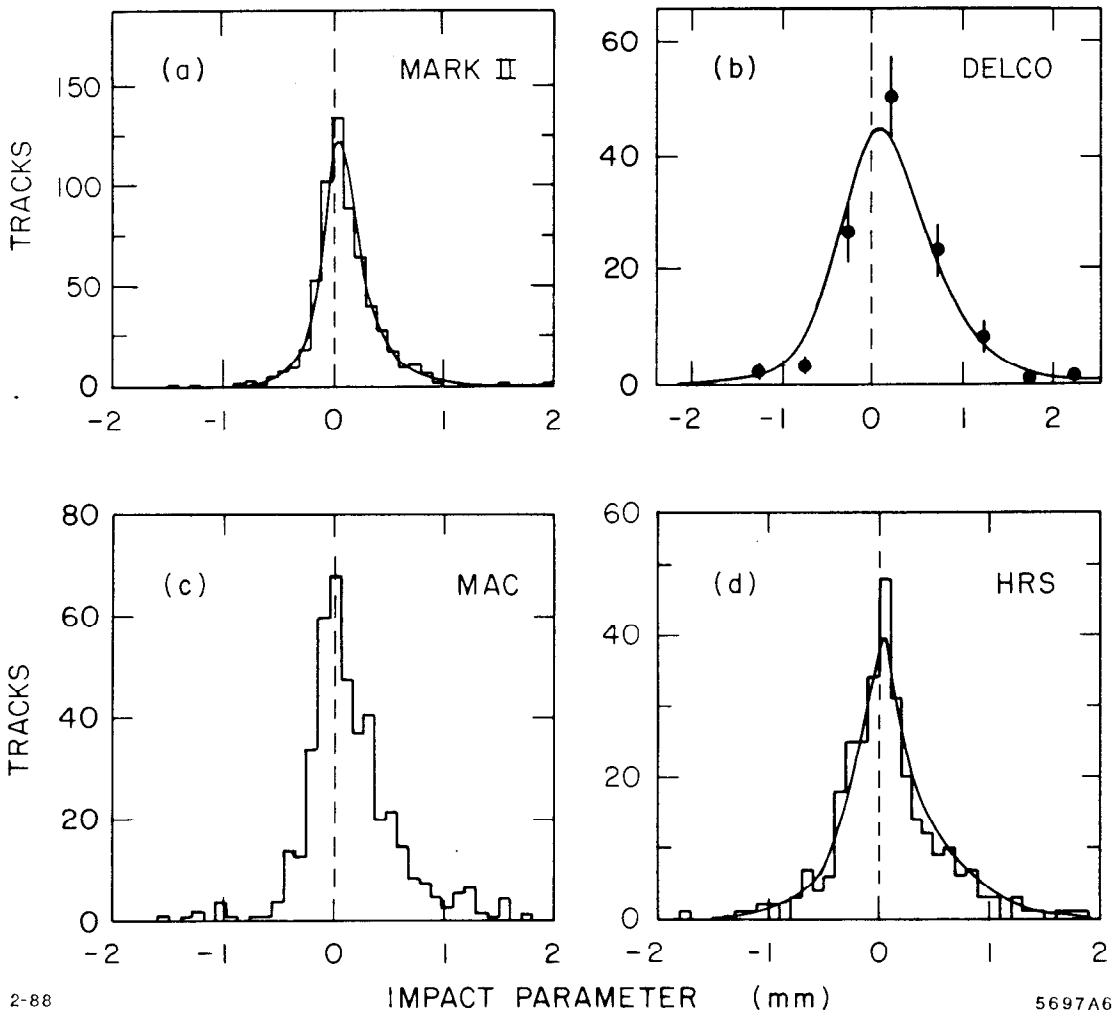

Fig. 24. Measurement of the beauty lifetime: Impact parameter distributions of the four PEP experiments.

and was operated at a pressure of 4 atmospheres. Each tube provided a position measurement with a resolution of 50 μm. The error on the impact parameter was improved from 350 μm for data recorded without the vertex chamber to 90 μm for the data with the vertex chamber. Multiple scattering contributed 360 μm/p(GeV) and 65 μm/p(GeV), respectively, to these errors. Hadronic events containing beauty particles were tagged by a muon or electron with a large transverse momentum, with respect to the thrust axis. The sample consisted of 462 events, 152 with the vertex chamber in operation, and is expected to contain 70% $b\bar{b}$ and 16% $c\bar{c}$ events. The impact parameters of all well-measured tracks with momentum above 0.5 GeV/c were measured in the plane transverse to the beam. There were 1558 and 441 tracks in the two data samples with impact parameters of less than 4 mm and 3 mm, respectively. The B production point was determined from remaining tracks in the event. This reduced the uncertainty in the impact parameter by about a

factor of three compared to the measurement relative to the beam center.

The more precise vertex chamber data show not only a positive displacement, but also a clear tail on the positive side. To provide a robust and precise measure of this distribution the mean is determined after 10% of the tracks are removed symmetrically from the tails. The trimmed means are 154 ± 20 μm for the early data and 129 ± 14 μm for the vertex chamber data. The B lifetime is obtained by adjusting its value in the Monte Carlo simulation to reproduce the measured trimmed mean, which is approximated by a sum of three contributions,

$$X_{meas} = f_b X_b + f_c X_c + f_{bg} X_{bg}.$$

The subscripts b, c, and bg refer to the beauty, charm and background tracks, respectively. f_i is the fraction of tracks from event type i, and X_i is the trimmed mean. The results are $\tau(B) = 1.24 \pm 0.29$ ps and $\tau(B) = 1.35 \pm 0.30$ ps, for the two subsamples, and for the total sample the lifetime is

$$\tau(B) = \{1.29 \pm 0.20(stat) \pm 0.07(syst)\} \cdot (1.00 \pm 0.15) \text{ ps}.$$

The complete electron sample yields 0.92±0.35 ps, while the muon data yield 1.30±0.25 ps. The systematic error has been separated into an additive term and an overall scale factor. The uncertainty in the trimmed mean X_b is mainly due to the uncertainty in the B fragmentation. The average energy of the B hadron is measured to be $< z >= 0.78 \pm 0.05$. The error on this quantity causes a 10% uncertainty in the overall scale. The uncertainty in the purity of the sample f_b arises from errors in the measured leptonic branching ratios, the b and c fragmentation, and detection efficiencies, it is estimated to contribute ±7%. The uncertainty in the determination of the B production point adds ±7% to the scale error. Present uncertainties in the lifetimes of the charm particles contribute only ±0.05 ps to the systematic error. By comparing the trimmed mean of the distributions rather than an the complete distributions bin by bin, the measurement becomes less sensitive to the exact shape of the resolution function and the background, in fact differences in the widths will have little effects, only asymmetric tails are important.

4.2.2 Mark II The Mark II group[78] has tripled the data sample since its first publication and has substantially reduced the systematic uncertainties. In particular, the inclusive lepton analysis has been repeated for a total sample of 4000 leptons, leading to a determination of the b quark fragmentation function with much improved precision. The final sample of 386 electron and 231 muons originates to $65 \pm 5\%$ from semi-leptonic B decay. To obtain an event by event measurement of the B production point, the jet vertex is determined from the best tracks in each event. It is then used to extrapolate along the thrust direction into the beam interaction region. The effects of the uncertainty in the thrust direction and the jet vertex errors are taken into account. Through a variety of checks in the data and

the Monte Carlo simulation, it has been shown that this procedure produces an unbiased estimate of the B production point. The precision on the impact parameter is improved by a factor of two by choosing the estimated production point over the beam centroid.

Rather than relying on isolated, high energy tracks in Bhahba events to derive the impact parameter resolution in hadronic events, the Mark II group has performed a detailed study of the detector performance and the resolution of charged particles tracks in jet-like hadronic events. In particular, they select tracks with a small fraction of transverse momentum in the xy plane, thereby reducing the effects of non-zero lifetime. The resolution in the impact parameters measured for these tracks is used in the fit of the lepton impact parameter distribution. This distribution (Figure 24a) contains 617 leptons and has a mean of 114.1 ± 12.5 μm. A maximum likelihood fit is used to extract the average B lifetime from this distribution. The fit assumes that each lepton comes from one of four possible sources: background, charm decay, beauty decay, and secondary charm decay in beauty decay. The fitting function represents a sum of each of these contributions,

$$P(\delta^i, \sigma_\delta^i, \tau_b, \tau_c) \;=\; f_{bg} P_{bg} + \sum_l f_l P_l(\delta^i, \sigma_\delta^i, \tau_b, \tau_c).$$

A likelihood function is defined as the product of the probability functions for individual events,

$$\mathcal{L}(\tau_b, \tau_c) \;=\; \prod_i P(\delta^i, \sigma_\delta^i, \tau_b, \tau_c)$$

with the average beauty and charm lifetime as free parameters. The relative contributions f_l and f_{bg} are derived from the lepton momentum spectra. The distribution functions for the background is measured. The charm and beauty contributions are taken from Monte Carlo simulations, but the multiplicity and the kinematics of semi-leptonic decays and the resolution functions are well understood. The impact parameter error is included in the fit to make use of its knowledge on an event by event basis. This reduces the effects of poorly measured track and enhances well measured tracks. As a result the overall error is roughly 30% smaller. The fit yields

$$\tau(B) = 0.98 \pm 0.12 \pm 0.13 \;\cdot\; ps.$$

The systematic error arises primarily from remaining the uncertainties in the detector resolution ($\pm$0.07 ps), the B contents of the sample ($\pm$0.08 ps), and the B fragmentation function ($\pm$0.05 ps) which is determined from the analysis of the inclusive lepton spectra.

4.2.3 DELCO The excellent electron identification of the DELCO experiment[79] leads to a very clean $b\bar{b}$ sample, and allows for a looser cut on the lepton transverse momentum, namely 1 GeV/c. The impact parameter for the 113 electron tracks is

measured relative to the beam centre, the average is 259 ± 49 μm. The B lifetime is determined from a maximum likelihood fit taking into account the measured resolution, including the non-Gaussian tails, the measured contributions from charm and background events in the sample, and the ± 3 mm cut on the impact parameter. The principal systematic errors arise from the uncertainty in the experimental resolution, $\pm^{0.07}_{0.04}$ ps, the fragmentation function and leptonic branching ratios, $\pm^{0.07}_{0.12}$ ps, and the Monte Carlo modelling of the jet axis, $\pm^{0.03}_{0.00}$ ps. The authors choose to add these errors linearly, leading to a result on the average B lifetime of

$$\tau(B) = 1.17 \pm {}^{0.27}_{0.22} \pm {}^{0.17}_{0.16} \cdot \text{ps}.$$

4.2.4 HRS The HRS group[80] bases its measurement on a sample of 312 high p_t electrons purity of $53 \pm 7\%$. The electron impact parameter distribution measured relative to the beam position (Figure 24d) has a mean of 80 ± 27 μm. The average B lifetime is determined from a maximum likelihood fit to the impact parameter distribution, which includes a free parameter to adjust the width of the assumed Gaussian resolution function. The result of the fit is:

$$\tau(B) = 1.02 \pm {}^{0.42}_{0.39} \cdot ps.$$

The error in this measurement represents the combined statistical and systematic errors. The dominant systematic errors are due to uncertainties in the B fraction and fragmentation function.

4.2.5 TASSO The TASSO collaboration[81] has presented a result based on the impact parameter measured of all charged particles in the event. This is an update on their B lifetime measurement using twice the number of events as previously published.[82] The group makes a cut on the boosted sphericity product, $s_1 \times s_2 > 0.18$, to increase the B contents in the two-jet events sample. The impact parameters of all well measured tracks are weighted by their track errors. A comparison of the measured mean of 86.8 ± 6.2 μm of all tracks with momenta above 1 GeV/c with the mean of Monte Carlo simulated distributions for different B lifetimes results in

$$\tau(B) = 1.52 \pm 0.18 \pm 0.24 \cdot \text{ps}.$$

In this measurement, less than 30% of the tracks originate from B decays, and most of them have smaller transverse momenta and impact parameters than the leptons selected by other experiments. The analysis relies totally on the Monte Carlo simulation to reproduce the effects of the track resolution, the composition of the event sample in terms of charm, beauty and background, and the charm and beauty fragmentation. In view of this, the quoted errors are surprisingly small.

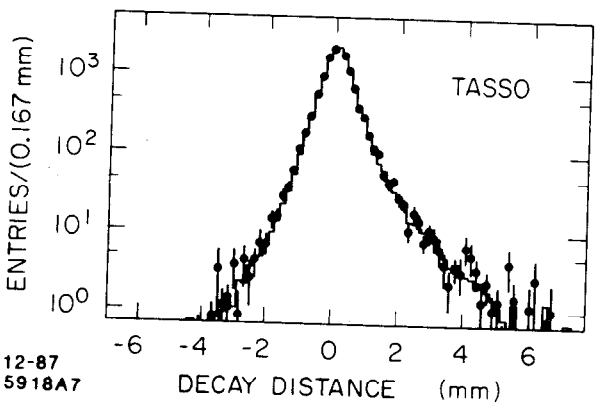

Fig. 25. TASSO: Decay length distribution for 15,364 selected vertices.

4.3 Secondary Vertex Measurements

4.3.1 TASSO Aside from the impact parameter technique, the TASSO experiment has explored two methods to determine the decay vertex and decay length of B particles. The three measurements are not independent, because they are based on the same 32,000 multi-hadron events recorded at a c.m. energy of 35 GeV, and the same Monte Carlo programs. For the two vertex methods, no particular cuts are applied to select $b\bar{b}$ events, all two-jet events are included in the sample. These measurements rely on a Monte Carlo simulation to reproduce the B decay multiplicities and fragmentation as well as the detector resolution and details of the track and vertex fitting. The main systematic errors stem from the uncertainties in this simulation.

In the first method, the events are divided into two jets by a plane perpendicular to the sphericity axis. In each hemisphere, the best 3-prong vertex is selected on the basis of the lowest χ^2. As illustrated in Figure 22b, the decay length is determined by using the sphericity axis as an estimate for the B direction. The most probable production point is determined by projecting the jet axis on to the beam envelope, taking into account the error in this direction. A number of cuts are imposed to reject poorly measured decay lengths. The decay length distribution for 15,364 vertices is shown in Figure 25, the mean is 83.7 ± 5.1 μm. A Monte Carlo prediction with the B lifetime and fragmentation function as free parameters is adjusted to fit the measured distribution. The fit yields

$$\tau(B) = 1.39 \pm 0.10 \pm 0.25 \cdot ps.$$

The same analysis applied to a sample of 2075 events that is selected by requiring that the boosted sphericity product exceed 0.18, gives an average distance of 175 ± 16 μm which translates to $\tau(B) = 1.35 \pm 0.16 \pm 0.27$ ps. The systematic error for both samples is dominated by the uncertainty in the fraction of B decays (± 0.17 ps) in the sample, the fragmentation function ($\pm^{0.10}_{0.11}$ ps) , the charm decay contents (± 0.09 ps), and uncertainties in the track and vertex reconstruction (± 0.09 ps).

In the second method, a common vertex of all track in each of the two jets is determined. In addition to the track error and angle, its rapidity is used as a weight to enhance to the contribution from high momentum tracks. A variable referred to as the dipole moment, ρ, is defined as the distance between the vertices of the two jets, projected onto the sphericity axis (Figure 22c). This measure of the decay length has the advantage that it does not require any reference to the production point. The measured distribution has a mean of 305±13 μm. The lifetime is estimated to be

$$\tau(B) = 1.37 \pm {}^{0.14}_{0.32} \pm 0.25 \text{ ps.}$$

The measurement of the dipole moment requires that both jet vertices are reconstructed. Consequently, the number of usable events is substantially smaller than for the single decay length measurement. This is the reason for the larger statistical error. Like for the previous measurement, the main uncertainty in this vertex technique is due to the complete reliance on Monte Carlo simulations to interpret the measured distributions. In additional to the uncertainties in the sample composition, one has to worry about the vertex determination for events that are known to contain multiple vertices. Also, the location of these global vertices is influenced by the fragmentation process and details of the track and event selection.

4.3.2 JADE The JADE group uses a general sample of approximately 30,000 multi-hadronic events recorded at c.m. energies of 35 GeV and 41.7 GeV. It also determines vertices with three or more tracks for each jet. For the 15,386 events with two good vertices, the dipole moment is determined. The authors use a weighting technique to distinguish a beauty enriched sample from the rest of the sample, including charm events. On the basis of the Monte Carlo generated distributions of the boosted sphericity product (Figure 21) each event is assigned a weight proportional to the probability that it represents a $b\bar{b}$ or background event. The distribution of dipole moments for the B weighted sample is shown in Figure 26. Trimming the tails by 4% of the sample on each side, results in a *trimmed* mean of 1010 ± 80 μm, as compared to a mean of the background weighted sample of 380±31 μm. This large difference is remarkable. A quantitative analysis is, however, by no means trivial. Monte Carlo events generated at different lifetime values are used to calibrate the dependence of the mean dipole moment on the B lifetime. The results is

$$\tau(B) = 1.46 \pm 0.19 \pm 0.30 \text{ ps.}$$

The systematic error comes largely from uncertainty in the fragmentation for charm, beauty, and light quarks, and from the method of vertex detection, including cuts made on the tracks and vertices, resolution uncertainties etc.. This result is still preliminary, it is presented here as another variant on the methods of determining decay vertices.

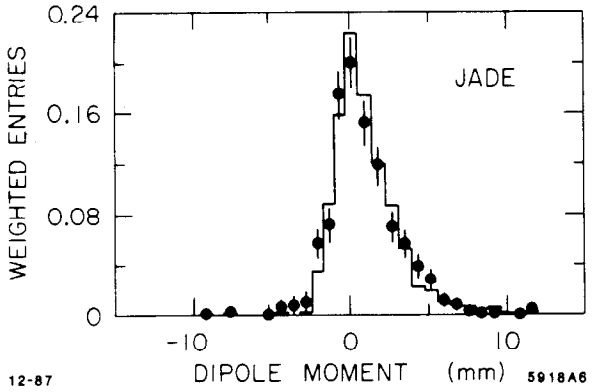

Fig. 26. JADE: Distribution of measured dipole moments for events weighted by the distribution of the sphericity product $s_1 \times s_2$to enhance $b\bar{b}$events. The histogram represents the Monte Carlo simulated distribution with $\tau(B) = 1.5$ ps.

4.4 Summary of the B Lifetime Measurements

A compilation of the six recent measurements of the average lifetime of B hadrons produced in e^+e^- annihilation is given in Table V. It is not obvious that the different experiment really measure the same quantity, since the measurements average over all beauty particles in the sample, and those samples may well have a different composition of particles. There is, however, no way to tell the difference, and therefore it will be ignored for now. The different measurements by the TASSO group are all based on the same data sample and thus are by no means independent. Only the results with the smallest error is listed in the table, the other measurements can be regarded as supporting evidence. The experiments agree very well, though the systematic errors remain substantial because of uncertainties in the sample purity, resolution, fragmentation and decay of B hadrons. Many features of the modelling of the hadronic final states are common among the experiments, as are some aspects of detector design and analysis, leading to errors that are not totally independent. The weighted average of the measurements (taken into account a common systematic error of 10%) is

$$\tau(B) = 1.18 \pm 0.14 \cdot 10^{-12} \text{ s}.$$

The only information on the lifetimes of individual B mesons has been obtained by the CLEO collaboration.[83] The number of observed di-lepton events in $\Upsilon(4s)$-decays translates to a limit $0.4 < \tau(B^0)/\tau(B^+) < 2.0$ at 90% confidence level.

The B lifetime measurement can be used determine the Cabibbo-Kobayashi-Maskawa matrix elements V_{cb} and V_{ub} which represent the coupling of the b quark to the charged weak current. The total decay rate can be derived from the measured semi-leptonic branching ratio of B mesons, $BR(B \to Xe\nu) = 11.4 \pm 0.5\%$[3] and a

Table V: Measurements of the Average Lifetime of Beauty Particles

	MARK II	MAC	DELCO	HRS	JADE	TASSO
Luminosity pb^{-1}	200	220	214	200	70	75
Vertex Chamber Inner Radius (cm)	10.1	4.8	12.1	9.0	9.9	8.1
ID Lepton e	Pb/LA	Pb/Gas	Cerenkov	Pb/Scint.	Pb/Glass	Pb/LA
μ	Fe	Magn. Fe			Fe	Fe
Cuts p (GeV/c)	2.0	2.0	1.0	2.0		
p_t (GeV/c)	1.5	1.5	1.0	1.5		
# Leptons	617	561	113	312		
Signal Fraction	0.65	0.70	0.79	0.53		
Resolution (μm)	84	87	150	100	160	100
Length (μm)	114±13	129±14	249±49	80±27	1080±80	84±5
Lifetime (10^{-12}s)	0.98 ± 0.12	1.24 ± 0.20	$1.17 \pm^{0.27}_{0.22}$	$1.02 \pm^{0.42}_{0.39}$	1.46 ± 0.19	1.39 ±0.10
Syst. Error	±0.13	±0.17	$\pm^{0.17}_{0.16}$		±0.30	± 0.25

theoretical estimate of the semi-leptonic decay rate,

$$\tau(B) = \frac{BR(B \to Xe\nu)}{\Gamma(B \to Xe\nu)} = \frac{C \cdot BR(B \to Xe\nu)}{\Gamma_0 \left[A \cdot |V_{cb}|^2 + |V_{ub}|^2\right]}.$$

The constant Γ_0 is proportional to the fifth power of the mass of the b quark. If we set m_b=5.0 GeV/c^2, we have

$$\Gamma_0 = \frac{G_F^2 m_b^5}{192\pi^3} = 7.14 \cdot 10^{-11} GeV = 1.09 \cdot 10^{14} s.$$

The coefficients A and C depend on the specific hadrons X contributing to the semi-leptonic decay rate. Several approaches have been chosen to calculate the numerical values of these coefficients, in agreement with the measured lepton spectra in beauty mesons. Altarelli *et al.*[84] have examined the lepton spectra in the context of the spectator model and compare the mass m_b to the well measured masses of the B mesons. They include the effects of soft gluon radiation and the Fermi motion within the meson. Another way to derive the semi-leptonic decay rate is to consider B decays rather than free quark decays. In such an approach, the matrix elements for exclusive decays are calculated and summed to obtain the total contribution. Wirbel, Bauer and Stech[85] have used a relativistic harmonic oscillator potential to derive the matrix elements for the hadronic current in the decay channels $B \to De\nu, D^* e\nu, \pi e\nu$, and $\rho e\nu$. More recently, Grinstein, Isgur, and Wise[86] derived the hadronic wave function from the non-relativistic solution of a potential which is a sum of a Coulomb and a linear term. These three different approaches to the calculation of the semi-leptonic B decay rate do not give identical

answers for the coefficient A and C. They agree rather well on the $b \to c$ transitions, but differ on the $b \to u$ rate. Clearly, more work is needed to improve these calculations. For now, we arbitrarily choose the result of the free quark calculation, A=0.5 and C=1.27, and assign an overall 25% error to account for the uncertainties in the rate calculations. Using the measured branching ratio of B mesons and the average B lifetime, one obtains

$$0.5 \cdot |V_{cb}|^2 + |V_{ub}|^2 \;=\; 1.13 \pm 0.14 \pm 0.30 \cdot 10^{-3},$$

where the first error represents the experimental, the second the theoretical uncertainties. Additional constraints on the ratio of the two matrix elements have been obtained from the CLEO and ARGUS experiments,

$$0.07 < |V_{ub}|/|V_{cb}| < 0.23.$$

The upper limit comes from the measurement of the endpoint of the lepton momentum spectrum in semi-leptonic B decay,[87] the lower limit is based on the observation of the decay modes $B \to p\bar{p}\pi, p\bar{p}\pi\pi$.[88] Under the assumption that this ratio is of the order of 0.15, one obtains

$$|V_{cb}| = 0.046 \pm 0.003 \pm 0.006.$$

With this additional input and the unitarity condition, the absolute values of all elements of the Cabibbo-Kobayashi-Maskawamatrix can be determined or severely constrained. In fact, the matrix becomes almost diagonal, and thus there is very little mixing between the second and the third generations of quarks.[89] The small value of $|V_{cb}|$ imposes constraints on the top mass, the ratio ϵ'/ϵ in K^0 decay and CP violation in beauty meson decay.

5. Conclusion

The present status of lifetime measurements of heavy flavour particles can be summarized as follows:

- Lifetimes of different charm particles are different,

  $$\tau(D^+) > \tau(D^0) \geq \tau(\Lambda_c).$$

  This observation clearly indicates problems with the naive parton description including short distance QCD effects and the need for W exchange and/or annihilation diagrams, and possibly effects from final state interactions. There is new information on many exclusive decays available from the Mark III and ARGUS experiments. In particular, the relatively large branching ratios for $D^0 \to \overline{K}^0\pi^0$ and $D^+ \to \Phi\pi^+$ suggest the absence of colour suppression. The large rate of $D^+ \to \overline{K}^0 K^+$ relative to $\overline{K}^0\pi^+$ could be explained by interference in D^+ decay and may be contributing to its reduced hadronic width.

- Six measurements at e^+e^- storage rings agree on an average lifetime of the B hadrons produced of (1.18 ± 0.14) ps. There is still only one directly observed, hadro-produced $B^-\overline{B}^o$ event.[69]

In summary, measurements of charm particle lifetimes have substantially improved over the last year, but orders of magnitude more data are needed to study lifetime of individual charm baryons and beauty mesons. The analysis of substantial amounts of new data from the fixed target experiments NA-32 , NA-14 and E-653 is still in progress. Also, there are several new experiments in preparation at CERN and Fermilab to study charm baryons and beauty mesons decay and production. The e^+e^- experiments ARGUS at DESY and CLEO at Cornell will continue for several years, but their measurements will be limited by systematic uncertainties.

At the SLC and LEP as well as the Tevatron collider, substantial production rates of charm and beauty particles are expected, and high precision vertex detectors are presently under construction. At colliding beam machines, the ultimate performance limits will not be set by the intrinsic resolution of the vertex detector, but by the multiple Coulomb scattering in the material of the vacuum pipe and the support structure. Thus the most important parameter will be the distance of the first detector from the beam interaction region. This in turn will be determined by the machine characteristics and the collimation and shielding to protect against radiation background. It appears improbable that detectors can be installed closer in radius than 4 cm at LEP and the Tevatron. Only at single-pass-colliders like the SLC will it be possible to place active detectors as close as 1 cm from the beam thus allowing for efficient vertex detection in three dimension. Such machines also operate with beams of much smaller dimensions, defining the interaction point to a few μm. In addition, plans are being made for the construction of dedicated high luminosity e^+e^- colliders to study beauty particles. Particular attention is given to tests of CP violation, many of which require the measurement of decay time dependent asymmetries. Without extremely precise vertex detectors and careful design of the interaction reagion, such tests will not be possible.

Thus, in the coming decade, we can expect a continued interest in the measurement of heavy quark lifetimes and couplings, hopefully including particles with *top* flavour.

It is an enormous effort, but it has been and will continue to be fun!

Acknowledgements

I should like to thank many of my friends and colleagues who contributed the results of many years of hard work to this review.

References

1. M. Kobayashi, T. Maskawa, Prog. Theor. Phys. **652**, 49 (1973).
2. R. H. Schindler in *Recent Results on the Charm Sector*, this volume
3. B. Gittelman and S. Stone in *B Meson Decay*, this volume
4. S. Petrera and G. Romano, Nucl. Instrum. Methods **174**, 61 (1980).
5. R. Sidwell, N.W. Reay and N.R. Stanton, Ann. Rev. Nucl. Part. Science **33**, 539 (1983).
6. C. Caso and M.C. Touboul, Riv. Nuovo Cim. **9**, No.12, 1 (1986).
7. J. Jaros, *Proceedings of the IV. International Conference on Physics in Collision*, Santa Cruz, CA, USA (1984)
8. K. Niu, E. Mikumo, and Y. Maeda, Prog. Theor. Phys. **46**, 1644 (1971).
9. N. Ushida *et al.*, Phys. Rev. Lett. **56**, 1767 (1986) and ibid. **56**, 1771 (1986).
10. M. Adamovich *et al.*, CERN/EP 86-77, and V. Castillo Gimenez, Thesis Doctoral, Universitad de Valencia (1986).
11. K. Abe *et al.*, Phys. Rev. **D33**, 1 (1985).
12. M. Aguilar-Benitez *et al.*, Phys. Lett. **122B**, 312 (1983).
13. A. Badertscher *et al.*, Phys. Lett. **123B**, 471 (1982).
14. M. Aguilar-Benitez *et al.*, Zeitsch. Physik **C3**, 491 (1986); and Phys. Lett. **193B**, 254 (1987).
15. K. Roberts, Ph.D. Thesis, University of Liverpool (1986).
16. M. Aguilar-Benitez *et al.*, Phys. Lett. **B189**, 254 (1987).
17. G. Bellini, L. Foa, and M. A. Giorgi, Physics Reports **84**, 9 (1982).
18. E. Belau *et al.*, Nucl. Instr. Meth. **217**, 224 (1983).
19. B. Hyams *et al.*. Nucl. Inst. Meth. **185**, 99 (1983).

20. J.T. Walker *et al.*, Nucl. Inst. Meth. **226**, 200 (1984).

21. G. Lutz *et al.*, MPI-PAE/Exp. El. 170 (1987)

22. P. Seller *et al.*, paper presented at the *IEEE Nuclear Science Symposium,* San Francisco (1987).

23. R. Bailey *et al.*, Nucl. Inst. Meth. **213**, 201 (1983).

24. S.R. Amendolia *et al.*, Nucl. Inst. Meth. **226**, 32 (1984).

25. E. Albini *et al.*, Phys. Lett. **110B**, 339 (1982).

26. S.R. Amendolia *et al.*, CERN-EP/87-20, submitted to Phys. Lett. (1987).

27. S.R. Amendolia *et al.*, Zeitsch. Physik **C36**, 513 (1987).

28. A. Filippas *et al.*, CERN-EP/87 211 (1987), presentation at the *Int. Symposium on the Production and Decay of Heavy Flavours*, Stanford (1987).

29. R. Bailey *et al.*, Zeitsch. Physik **C28**, 357 (1985).

30. H. Becker *et al.*, Phys. Lett. **184B**, 277 (1987).

31. H. Palka *et al.*, Zeitsch. Physik **C35**, 151 (1987).

32. S. Barlag *et al.*, Zeitsch. Physik **C37**, 17 (1987).

33. H. Becker *et al.*, Phys. Lett. **184B**, 277 (1987).

34. S. Barlag *et al.*, Phys. Lett. **184B**, 283 (1987).

35. S. Barlag *et al.*, Contribution to the *Int. Symposium on Lepton and Photon Interactions at High Energies*, Hamburg (1987).

36. J.C. dos Anjos *et al.*, Phys. Rev. Lett. **58**, 311 (1987), and ibid. **58**, 1818 (1987).

37. J.R. Raab *et al.*, Fermilab-PUB-87/144E (1987), Submitted to Phys. Rev. D.

38. J.C. Anjos *et al.*, Fermilab-Pub-87/142E (1987).

39. Particle Data Group, Rev. Mod. Phys. **56**, 1 (1984).

40. S. Biagi *et al.*, Phys. Lett. **122B**, 455 (1983), and ibid. **150B**, 230 (1985).

41. S. Biagi *et al.*, Zeitsch. Physik **C31**, 33 (1986).

42. P. Coteus *et al.*, Phys. Rev. Lett. **59**, 1530 (1986).

43. H.L. Lynch in *Detectors for e^+e^- Experiments*, this volume.

44. H. Yamamoto *et al.*, Phys. Rev. **D22**, 2901 (1985).

45. L. Gladney *et al.*, Phys. Rev. **D34**, 2601 (1986).

46. S.R. Wagner *et al.*, Phys. Rev. **D36**, 2850 (1987).

47. S. Abachi *et al.*, ANL-HEP-CP-86-73, ANL-HEP-CP-8662, ANL-HEP-CP-87-60. Contributions to the *Int. Conference on High Energy Physics*, Berkeley, (1986).

48. S. Abachi *et al.*, Phys. Rev. Lett. **56**, 1775 (1986).

49. M. Althoff *et al.*, Zeitsch. Physik **C32**, 343 (1986).

50. W. Braunschweig *et al.*, Zeitsch. Physik **C35**, 317 (1987), and Contribution to *Int. Symposium on Lepton and Photon Interactions at High Energy*, Hamburg (1987).

51. S.E. Csorna *et al.*, Phys. Lett. **B191**, 317 (1987).

52. H. Albrecht *et al.*. Contribution to the *International Symposium on Lepton Photon Interactions at High Energy*, Hamburg (1987).

53. R.M. Baltrusaitis *et al.*, Phys. Rev. Lett. **54**, 1976 (1985).

54. E.N. Vella *et al.*, Phys. Rev. Lett. **48**, 1515 (1982).

55. M.K. Gaillard, B.W. Lee, and J.L. Rosner, Rev. Mod. Phys. **47**, 277 (1975).

56. B. Guberina, *et al.*, Phys. Lett. **89B**, 111 (1979).

57. M. Bander *et al.*, Phys. Rev. Lett. **44**, 7 (1980).

58. H. Fritzsch and P. Minkowski, Phys. Lett. **90B**, 455 (1980).

59. R. Rückl, Habilitationsschrift, München (1983).

60. M. B. Shifman and M.A. Shifman, Sov. J. Nucl. Phys. **41**, 120 (1985), and ibid. **64**, 698 (1986).

61. M. Bauer, B. Stech, and M. Wirbel, Zeitsch. Physik, **C34**, 103 (1986).

62. A.J. Buras, J.-M. Gérard, and R. Rückl, Nucl. Phys. **B268**, 16 (1986).

63. H. Albrecht *et al.*, Phys. Lett. **158B**, 525 (1985).

64. C. Bebec *et al.*, Phys. Rev. Lett. **56**, 1983 (1986).

65. R.M. Baltrusaitis *et al.*, Phys. Rev. Lett. **56**, 2136 (1986).

66. J.F. Donoghue, Phys. Rev. **D33**, 1516 (1986).

67. B. Guberina, R. Rückl, and J. Trampetic, Zeitsch. Physik **C33**, 297 (1986).

68. J.K. Körner *et al.*, Zeitsch. Physik **C2**, 117 (1979).

69. J. P. Albanese *et al.*, Phys. Lett. **158B**, 186 (1985).

70. E. Fernandez *et al.*, Phys. Rev. Lett. **51**, 1022 (1983).

71. N.S. Lockyer *et al.*, Phys. Rev. Lett. **51**, 1316 (1983).

72. M. E. Nelson *et al.*, Phys.Rev. Lett. **50**, 1542 (1983).

73. E. Fernandez *et al.*, Phys. Rev. Lett. **50**, 2054 (1983).

74. D.E. Koop *et al.*, Phys. Rev. Lett. **52**, 970 (1984).

75. R. A. Ong *et al.*, SLAC-PUB-4550, submitted to Phys. Rev. Lett. (1988).

76. R. Ong, Ph.D. Thesis, SLAC-320 (1987).

77. W.W. Ash *et al.*, Phys. Rev. Lett. **58**, 640 (1986).

78. R. Ong et al. SLAC-PUB-4559 (1988), submitted to Phys. Rev. Lett.

79. D.E. Klem *et al.*, SLAC PUB-4025 (1986), submitted to Phys. Rev. D.

80. J.M. Brom *et al.*, Phys. Lett. **195B**, 301 (1987).

81. W. Braunschweig *et al.*, Contribution to the *Int. Symposium on Lepton Photon Interactions at High Energy*, Hamburg (1987).

82. M. Althoff *et al.*, Phys. Lett. 149B (1984) 524.

83. A. Bean *et al.*, Phys. Rev. Lett. **58**, 183 (1987)

84. G. Altarelli *et al.*, Nucl. Phys. **208**, 365 (1982).

85. M. Wirbel, B. Stech, and M. Bauer, Zeitsch. Physik **C29**, 637 (1985).

86. B. Grinstein, M. B. Wise, and N. Isgur, Phys. Rev. Lett. **56**, 298 (1986)

87. S. Behrends *et al.*, **59**, 407 (1987).

88. W. Schmidt-Parzefall, Proceedings of the *Int. Conference on Lepton and Photon Interactions at High Energy*, Hamburg 1987.

89. K. Kleinknecht and B. Renk, Zeitsch. Physik **C34**, 209 (1987).